

Department of Physics, Chemistry and Biology

Final Thesis

Growth of GaN on lattice matched AlInN substrates

**Reem Omer Rahmatalla
Muhammad Boota**

LiTH-IFM-A-EX-08/1924-SE



**Linköping University
INSTITUTE OF TECHNOLOGY**

Department of Physics, Chemistry and biology
Linköpings University
SE-581 83 Linköpings, Sweden

Abstract

This project was planned in order to study the effect of growth and crystalline quality of GaN on lattice matched $\text{Al}_{1-x}\text{In}_x\text{N}$ seed layer. The GaN lattice matched $\text{Al}_{0.81}\text{In}_{0.19}\text{N}$ seed layer was grown by co-sputtering of Al and In target using only N_2 as a sputtering gas in a direct current (DC) reactive magnetron sputter deposition chamber under UHV conditions at low temperature (230°C) on different substrates. The Indium composition was calculated using Vegards law from lattice parameters determined by XRD. The Indium composition was determined by Rutherford Backscattering Spectroscopy (RBS) as well. X-rays diffraction (XRD) showed high crystalline quality wurtzite hexagonal $\text{Al}_{1-x}\text{In}_x\text{N}$ seed layers grown at this temperature. The GaN was grown on top of $\text{Al}_{0.81}\text{In}_{0.19}\text{N}$ seed layer by halide vapour phase epitaxy (HVPE) using a mixture of N_2 and H_2 and only N_2 as a carrier gas in order to study the effect of carrier gas on crystalline quality of GaN. The GaN films were characterised by high resolution X-rays diffraction (HRXRD), scanning electron microscopy (SEM), cathode luminescence (CL) and high resolution transmission electron microscopy (HRTEM) in order to study stress, strain, crystalline quality, surface morphology and optoelectronic properties in relation with the defect density and the microstructure of grown GaN films.

Acknowledgements

- We would like to express our deep gratitude to our supervisors, Prof. Jens Birch and senior researcher Carl Hemmingsson for giving us opportunity to do this project under their supervision. We are greatfull to our supervisors for their confidence, patience and kindness which they exhibited towards us.
- We would like to thanks Assistant Professor Fredrik Eriksson for helping us during X-rays reflectivity measurements.
- We would like to thanks Carina Höglund (PhD student) and Muhammad Junaid (PhD student) for RBS measurements. We would also like to thanks Carina Höglund (PhD student) for helping us during growth of $\text{Al}_{0.81}\text{In}_{0.19}\text{N}$ seed layer, XRD measurements and Muhammad Junaid (PhD student) for helping us during growth of $\text{Al}_{0.81}\text{In}_{0.19}\text{N}$ seed layer, XRD measurements and TEM sample preparation.
- We would like to thanks Docent. Per Person for helping us during HRTEM measurements.
- We would like to thanks senior researcher Galia Pozina for helping us in CL measurements.
- We would like to thanks Director of studies “International Master programme in Materials Physics and Nanotechnology” Prof. Leif I. Johansson for his kind support, care and guidance during entire master programme.
- I (Muhammad Boota) have no words to thanks my parents, my brothers, my sisters for their love, encouragement and prayers during my entire study period. I also have no words to thanks to my wife and kids for their love and sacrifice.
- I (Muhammad Boota) have no words to say thanks to my brother like friend Col. Khalid Masood Sheikh for his encouragement and support for my entire master programme. I would also like to thank to my very nice friend Khurram Shahzad for his support and encouragement.
- I (Muhammad Boota) would like to thanks to all Pakistani friends for being helpful, friendly and cooperative during my entire stay in Linköpings, Sweden.
- I (Reem Omer Rahmatalla) would like to thanks my parents for their continuous support, their love, prayers, and for believing that I will do it.
- I (Reem Omer Rahmatalla) would like to say many thanks to Asim my husband, for his love and generous support, for learning me how to study and encouraging me to catch the most difficult dreams. I will keep remembering his words (NEVER GIVE UP).
- I (Reem Omer Rahmatalla) would like to thanks to my kids Mohamed and Omer for being patient at the tough time during my study, their smiles are real supporting power. I LOVE YOU BOTH.
- I (Reem Omer Rahmatalla) would like to thanks my brother, my sisters for being around always.

My thanks will be at the beginning and the end to ALLAH my God who said:

... (And when your Lord made it known: If you are grateful, I would certainly give to you more)...
(14:7)

Table of Contents

Chapter 1: Introduction.....	1
1.1 Introduction.....	1
1.2 Thesis objective.....	1
1.3 Material properties.....	2
1.3.1 Group III nitride properties.....	2
1.3.2 Energy band structure.....	3
1.3.3 Crystal structure.....	4
1.4 Role of different layers.....	5
1.5 Growth modes.....	6
1.5.1 Island growth mode (Volmer-Weber).....	6
1.5.2 Layer-by-layer growth (Frank-van der Merwe).....	6
1.5.3 Stranski-Krastanow growth mode.....	6
Chapter 2: Growth Techniques.....	7
2.1 Reactive magnetron sputtering epitaxy (RMSE).....	7
2.1.1 Deposition Chamber.....	8
2.2 Halide vapour phase epitaxy (HVPE).....	10
2.2.1 Chemistry.....	10
2.2.2 Reactor Design.....	11
Chapter 3: Characterisation Techniques.....	13
3.1 X-Ray Diffraction (XRD).....	13
3.1.1 X-Ray Generation.....	13
3.1.2 Bragg's Law.....	14
3.1.3 Reciprocal space mapping (RSM).....	15
3.2 Transmission Electron Microscopy (TEM).....	16
3.2.1 TEM sample preparation.....	18
3.3 Cathodoluminescence (CL).....	18
3.4 Optical Microscope (OM).....	18
Chapter 4: Experimental details and characterisation of $\text{Al}_{1-x}\text{In}_x\text{N}$ seed layer.....	20
4.1 Sample preparation.....	20
4.1.1 Wafer cutting.....	20
4.1.2 Cleaning process of samples.....	20
4.1.3 Cleaning process of sample holders.....	21
4.2 Magnetron Sputter Deposition of TiN buffer and $\text{Al}_{1-x}\text{In}_x\text{N}$ seed layers.....	21
4.2.1 De-gassing of samples.....	21
4.2.2 Growth of TiN buffer layer.....	21
4.2.3 Growth of $\text{Al}_{1-x}\text{In}_x\text{N}$ seed layer.....	23
4.2.4 Summary of grown samples during composition tuning.....	26

4.3 HVPE Growth of thick layer of GaN.....	26
Chapter 5: Results and Discussions.....	28
5.1 Optical microscope (OM) results.....	29
5.2 X-Ray diffraction (XRD) results.....	34
5.1 Transmission electron microscope (TEM).....	41
5.2 Cathode luminescence (CL) and SEM results.....	44
Chapter 6: Conclusions.....	49
Chapter 7: References.....	50

Chapter 1: Introduction

1.1 Introduction

The preparation of nitrides has been reported since at least 1928, and AlN, and GaN were in fact the first nitride semiconductors ever described [1.1]. The first AlN crystals were grown in 1915 by sublimation of AlN in N₂ atmosphere, while the first reports on the synthesis of InN using traditional chemical methods date from the 1970s [1.2]. In 1932 the first GaN was produced in the powder form [1.3]. Epitaxial GaN was first produced by Maruska and Tietjen in 1969 using Halide Vapour Phase Epitaxy (HVPE) [1.4]. The first GaN were grown below 600C to prevent decomposition. However, these layers were polycrystalline. By raising the temperature to 950C better quality single crystal layers of GaN were fabricated [1.5]. Metal-organic chemical vapour deposition technique (MOCVD) was introduced for depositing GaN in 1971[1.4]. However, the crystal quality was poor due to the large lattice mismatch between the GaN and the sapphire. This problem was overcome in 1985 when Amano et al introduced AlN seed layers prior to the GaN [1.3]. The big step in III-nitride research was the achievement of good P-type conductivity by Mg doping followed by either low-energy electron beam irradiation or high-temperature annealing in N₂ atmosphere [1.2]. High-power LDs were fabricated using epitaxially lateral overgrown GaN (ELOG) and GaN quasi substrates [1.2], the (ELOG) technique has been reported to reduce the dislocation density of GaN. After that the progress of manufacturing devices based on group III nitride was accelerated. In 2002, Nichia Cororation announced the development of high power InGaN LED'S for white, blue, and green light emission with expected lifetime of 100 000 h [1.4]

1.2 Thesis objective

The growth and fabrication of devices based on GaN is done on foreign substrates since substrates of GaN are not commercially available yet, therefore the objective of this study is to grow thick Halide Vapour Phase Epitaxy (HVPE) GaN on a foreign substrate (hetroepitaxy) material such as Sapphire on a lattice matched AlInN seed layer.

The growth on a foreign material creates a high density of defects such as misfit dislocation and even cracks due to biaxial stress. These defects will reduce the lifetime and performance of the devices. In order to overcome these problems, Al_{1-x}In_xN seed layers with different thickness and a composition that gives lattice parameters matched to the GaN were proposed as a seed layer to be deposited before the GaN.

Varying of the $\text{Al}_{1-x}\text{In}_x\text{N}$ layers thickness was done in order to study how it affects the crystal quality of the GaN. This required structural characterization of AlInN epilayers and thick HVPE GaN.

1.3 Material properties

1.3.1 Group III nitride properties

Group three (III) nitride semiconductors (GaN, AlN, InN) are recognized as some of the most promising materials for fabricating optoelectronics devices operating from infrared to deep ultra-violet spectral region due to their unique physical properties such as the wide direct band-gap, high charge carrier mobility, and high melting temperatures comparing to GaAs and Si thus making them more stable for electronic devices to be operated at high temperatures or in high power devices [1.4].

GaN is combined with AlInN to fabricate devices high frequency, and also in optoelectronic application as light-emitting diodes in the visible and ultra-violet region. GaN has a high melting point coming from the strong bonds between the Ga and N. It is a stable material which is insoluble in water at room temperature. These properties of GaN made it an attractive material for protective coatings as well. Growth of group III nitride alloys is difficult due to the large immiscibility and difference in the thermal stability between AlN and InN [1.6], which means that it is impossible to grow $\text{Al}_{1-x}\text{In}_x\text{N}$ by processes which require high temperatures. Therefore, it is best to grow such alloys at low temperatures with growth techniques such as Plasma Assisted Molecular Beam Epitaxy (PAMBE) or Magnetron Sputtering Epitaxy (MSE) [1.7].

Table (1.1) shows some physical properties of group III nitrides and some other semiconductors materials, [1.4,1.10].

Material	Symmetry	Energy gap (eV)	Melting point (°C)	Lattice constants (Å)	e- mobility (Cm²/Vs)	Therm.exp. Coeff.[10⁶/k]
GaN	Wurtzite	3.43	2500	a: 3.19	1000	a: 5.59
	Hexagonal			c: 5.19		c: 3.17
AlN	Wurtzite	6.2	2275	a: 3.11	1100	a: 4.2
	Hexagonal			c: 4.98		c: 5.3
InN	Wurtzite	0.7	1925	a: 3.53	2700	a: 3.83
	Hexagonal			c: 5.69		c: 2.75

6H-SiC	Hexagonal	3.0	2830	a:3.08 c:15.12	370a 50c	a: 4.2 c:4.7
Diamond	Diamond cubic	5.45	4700	3.56	1900	1.5
Si	Diamond cubic	1.12	1415	5.43	1350	2.56
GaAs	Zincblende cubic	1.43	1238	5.65	8500	6.8
Sapphire	Hexagonal	2040	2040	a:4.758 c: 12.991	X	a: 8.11 c: 7.28
MgO	Cubic	2800	2800	4.216	X	a:8.0
MgAl₂O₄	Cubic	2130	2130	8.083	X	a:7.45

1.3.2 Energy band structure

The ternary nitride Al_{1-x}In_xN consists of two binary nitrides and has a wide band-gap ranging from 0.7 for InN to 6.2eV for AlN. The energy band gaps in the nitride group is direct, which means band to band transition can occur at the Γ point in the E - k diagram without phonon involvement [1.4]. Engineering of this ternary alloy of AlN and InN makes it possible to match the lattice parameters with GaN. Some research groups have reported that Al_{1-x}In_xN composition with (x=0.17) gives the same a lattice parameter as GaN [1.8, 1.9].

Figure (1) shows the band-gaps versus lattice constants for several wide band gap semiconductors and other semiconductors at room temperature. The solid lines show the possible path of group III nitride ternary alloy.

The linear relationship between the band gaps and molar fraction for a ternary semiconductor B_xA_{1-x}N that is composed of the binary constituents AlN and BN is given in equation [1.1].

$$E_g(AN)(1-X) + E_g(BN)X = E_g(ABN) \quad [1.1]$$

Where X is the molar fraction of BN, $E_g(AN)$, $E_g(BN)$, $E_g(ABN)$ are the Energy band gap of the two constituents and the resulting alloy respectively.

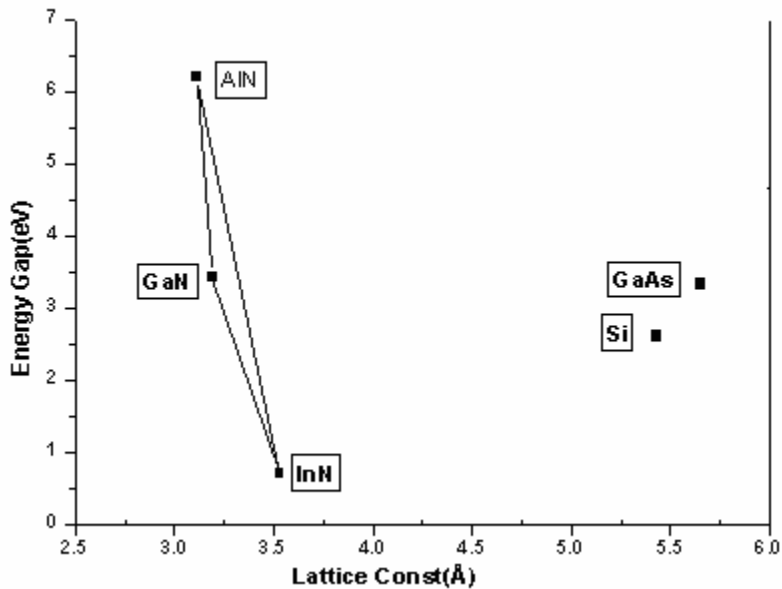


Fig.1.1. Energy band gap Vs lattice constant for different materials.

1.3.3 Crystal structure

Group III nitride can be in one of three possible crystal structures, rock salt, Zink-blende (cubic) and wurtzite (hexagonal). Among these, wurtzite is the most thermodynamically stable structure and the binary group three nitrides will all naturally crystallize into a hexagonal wurtzite structure [1.4.] In case of ternary alloys of AlN and InN the structure will also gives wurtzite structure, in which some In atoms have been replaced by Al atoms or vice versa.

In this study a buffer layer of TiN was deposited on top of the sapphire substrate and the AlInN seed layer was deposited on top of the TiN. Finally, GaN was grown on the AlInN seed layer. TiN has a cubic (111) crystal structure and the sapphire substrate has a (0001) hexagonal wurtzite structure. Both the GaN and the AlInN seed layer have hexagonal wurtzite structure. The cubic (111) and the hexagonal (0001) planes both have hexagonal surface symmetries, therefore, GaN can be grown hetero-epitaxially with a high structural order on the sapphire, and a single crystal wurtzite structure can be obtained.

Fig 1.2 shows the wurtzite structure unit cell. In this structure there are four atoms per unit cell, two nitrogen and two group three elements. The wurtzite structure is asymmetric along the c-axis which means that the directions of the bonds are different along [0001] and [000-1], this asymmetry gives rise to polarisation of the film [1.10].

The primary polar plane (0 0 0 1) for the wurtzite structure is called Ga- polar if the film ends with a Ga atom layer, and N-polar (0 0 0 -1) polar if it ends with a nitrogen atomic layer [1.10]

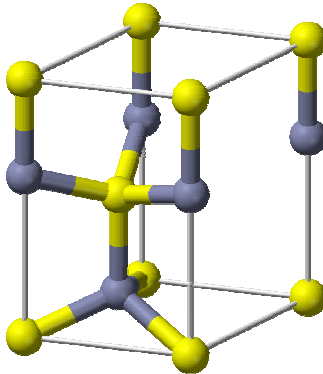


Fig 1.2. The crystal structure of the hexagonal wurtzite unit cell.

1.4 Role of different layers

Seed layers or buffer layers are intermediate layers which are deposited before the nitride in order to improve the quality of the GaN thick layer and to overcome substrates related problems such as impurity diffusion, misfit dislocations, stacking mismatch boundaries and biaxial stress [1.4]. The foreign substrates are used because there is a lack of less expensive commercial bulk GaN substrates with different thicknesses.

Table (1.2) shows some of the problems arising from heteroepitaxy growth. In this work $\text{Al}_{1-x}\text{In}_x\text{N}$ seed layers were grown prior to the GaN to enable the GaN to start the growth on top of a lattice matched nitride thin film with small lattice mis-match instead of starting the growth immediately on the substrates with large lattice mis-match. This facilitates the nucleation and decreases the formation of defects.

TiN has been chosen as a buffer layer prior to the AlInN thin film. It has metallic properties. The used substrates MgO, Sapphire and Spinal are transparent, so by introducing the metallic seed layer, the temperature of the group III nitride growth surface increases by better IR absorption, which cause a higher mobility at the surface and lead to epitaxial film growth.

Table (1.2): Problems arising from the growth on top of a foreigner substrate, data collected from Ref [1.4,1.10].

Substrate Properties	Resulting Problems
a- lattice constant mismatch	High misfit dislocation
c-lattice constant mismatch	Anti-phase boundaries, inversion Domain boundaries
Thermal expansion coefficient mismatch	Biaxial stress, formation of crack in the film and the substrate

1.5 Growth modes

At the nucleation stage, the film starts to grow in one of the three basic growth modes which observed from the film formation. The different growth modes are illustrated in Fig 1.3.

1.5.1 Island growth mode (Volmer-Weber mode)

The island growth mode, also known as three-dimensional growth, occur when the adatoms forms clusters, and these clusters nucleate on the substrate and grow to form islands. In this growth mode the bond between the adatoms is stronger than the bond between the adatoms and the substrate surface.

1.5.2 Layer-by-layer growth (Frank-van der Merwe)

Two-dimensional growth occurs when the extension of the smallest stable nucleus occurs overwhelmingly in two dimensions. It results in the formation of planar sheets [1.11]. In this growth mode, the bond between the adatoms and the substrate is stronger than the bond between the adatoms. This growth is most often realized for lattice-matched combinations of semiconductor materials with high interfacial bond energies.

1.5.3 Stranski-Krastanow growth mode

Stranski-Krastanow growth mode is a combination of a 2D layer followed by reorganization of the surface material in which 3D islands are formed. In this growth the film starts to grow layer by layer mode, after completing one or more monolayers this growth mode becomes unfavourable and the film continue its growing in island growth mode. The lattice mis-match between the film and the substrate induces a strain in the film and this could be one of the reasons for the transition from 2D to 3D growth mode.

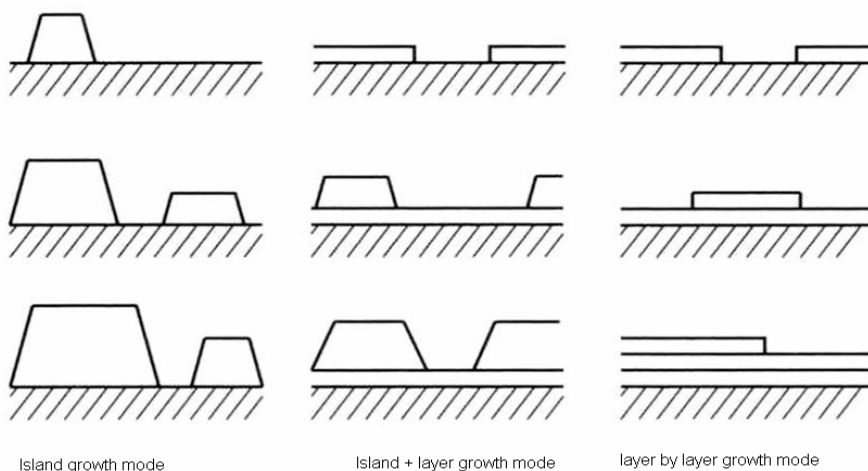


Fig 1.3.The different growth modes: island growth mode, island +layer growth mode, and layer-by-layer growth mode.

Chapter 2: Growth Techniques

Thin film growth techniques are usually divided into two groups.

1. Physical Vapour Deposition (PVD)
2. Chemical Vapour Deposition (CVD)

In the first part of this project (Growth of AlInN), we utilised reactive magnetron sputter deposition, which refer to physical vapour deposition (PVD) and in the second part of this project (Growth of GaN on top of AlInN layer), we utilised halide vapour phase epitaxy which refer to chemical vapour deposition (CVD).

2.1 Reactive Magnetron Sputter Epitaxy

The word Epitaxy consists of the two Greek words “Epi” and “Taxis”. The word “Epi” means placed or resting upon and “Taxis” means arrangements. From this we can define Epitaxy as growth of single crystal film on top of a crystalline material [2.1]. MSE is epitaxial growth by reactive magnetron sputter deposition under the same stringent vacuum and sample handling conditions as is practice in molecular beam epitaxy (MBE) [2.2].

The high purity and high structural quality of the grown material demands ultra high vacuum (UHV), low background pressure, high purities of working gas and sources etc [2.2].

The magnetron sputter deposition technique is based on gas phase transport of species, which are going to be deposited onto a substrate. The metallic target is bombarded with high-energy ions generated in glow discharge plasma and the atoms from the surface layer of the target materials are ejected due to momentum transfer of the ions. The sputtering gas may be pure noble gas, typically Ar, or diluted with a reactive gas such as nitrogen. In reactive sputtering, the gas is made to react with the metallic target atoms at the substrate surface to form the required molecules on the surface. In some cases, a layer of molecules formed on the target surface can cause decreased sputtering yield and a decrease of the sputtering rate. To avoid this problem, the reactive gas can be mixed with a noble gas like Ar.

In this study, we have used direct current (DC) magnetron sputtering which gives a higher deposition rate as compared to simple DC sputtering. In magnetron sputtering, permanent magnets are placed behind the metallic target. The magnets may have a shape of a rectangle or circular ring depending upon the shape of the target. The field of the permanent magnets confine the electrons and the generated plasma close to the surroundings of the target surface [2.1]. Due to the magnetic field created by the magnet placed behind the target, the electron path extends due to a rotational motion. That increases the degree of ionization because of a greater collision probability. Thus the ion/electron density increases in front of the target. Ions are accelerated due to force of attraction by the negatively biased target. When these accelerated ions collide with the target surface, they cause ejection of target atoms due to momentum transfer. The schematic cross section of a so called balanced and an unbalanced magnetron is shown in fig.1. The balanced magnets have identical magnetic field strength and the unbalanced magnets have non-identical strength due to identical and non-identical coupling of magnetic lines of forces between the central pole piece and the outer pole piece, respectively. In this project, we

have used a central piece and outer circular ring shaped type II unbalanced magnetron. The unbalanced magnetrons have some advantages over the balanced magnetrons. For example

- Unbalanced magnetrons can raise plasma density at the substrate from 10^6 - 10^8 cm $^{-3}$ range to the 10^8 - 10^{10} cm $^{-3}$ range.
- Unbalanced magnetron promotes the ion bombardment for the desired modification of the growing films [2.1].

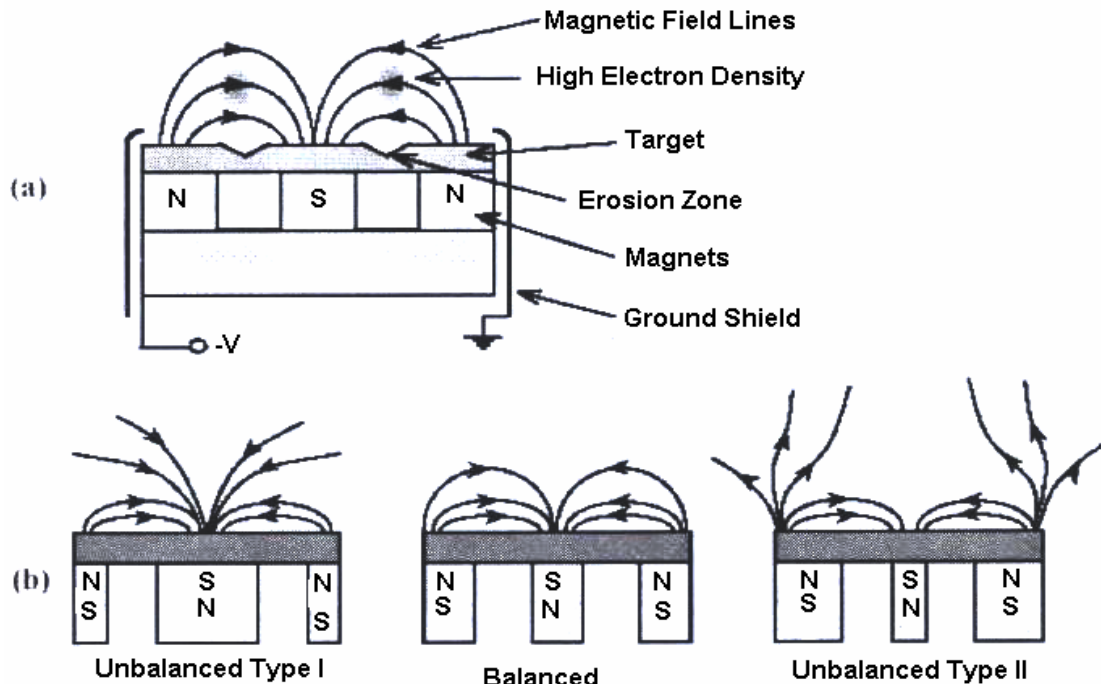


Fig.1. (a) Systematic cross section of a magnetron showing magnetic field lines and the created erosion zone on the target. (b) Balanced and unbalanced type I and type II magnetron configurations with magnetic field lines. [2.3]

2.1.1 Deposition Chamber

The sputtering system “Ragnarök” which is used in this project is made up of a stainless steel ultra high vacuum (UHV) chamber which is all metal sealed and water-cooled. The UHV deposition system “Ragnarök” is shown in fig. 2. In this system a base pressure of 5×10^{-10} torr can be achieved after baking at 200 °C for 48 hours by using a 1000 litre / minute turbo molecular pump (TMP) which is backed by a molecular pump. A titanium sublimation pump surrounded by liquid nitrogen cooled shroud is also connected to the UHV chamber that can be used during operation to keep residual gases at minimum level. Nitrogen and hydrogen are main contribution to the background pressure with minor traces of CO₂, Ar and Kr. That can be detected by a mass spectrometer, which is permanently connected to the system.

The system is also equipped with three different working gases that are N₂, Ar and Kr. The gases are cleaned up to 99.99999 % by special gas purifiers in order to assure low level residual gas contents even during the sputtering when the total pressure in the chamber is in the mille Torr range. The highly purified gases are allowed to enter in to the chamber by mass flow controllers (MFCs) in a baked all stainless steel manifold with UHV compatible seals.

The pumping system connected with the chamber can provide a stable working gas pressure about five mTorr. That can be increased by using a so-called baffle. A capacitance monometer connected with the system measures the absolute pressure of the working gas. That gauge measures pressure independent of the nature of the gas.

The bottom flange of the system is equipped with four sources with central piece and outer ring shaped type II magnetrons. Among these four sources two are 50 mm in diameter and two are 75 mm in diameter. These sources are simultaneously positioned toward a common focal point that is located 15 cm away from the sources and make 30° angle with the vertical axes of the chamber. During deposition, the substrate is kept at this common focal point.

Substrates, up to 2 inch in diameter, can be mounted in the sample holder of this system. The sample holder can move in three dimensions in order to bring the substrate in the focal point of the sources. The sample holder can be rotated around its axis up to 120 rpm in order to get a uniform deposition during the growth process. This system is equipped with substrate heater and the temperature of the substrate can be measured by a thermocouple sitting on the backside of the substrate [2.2,2.3].

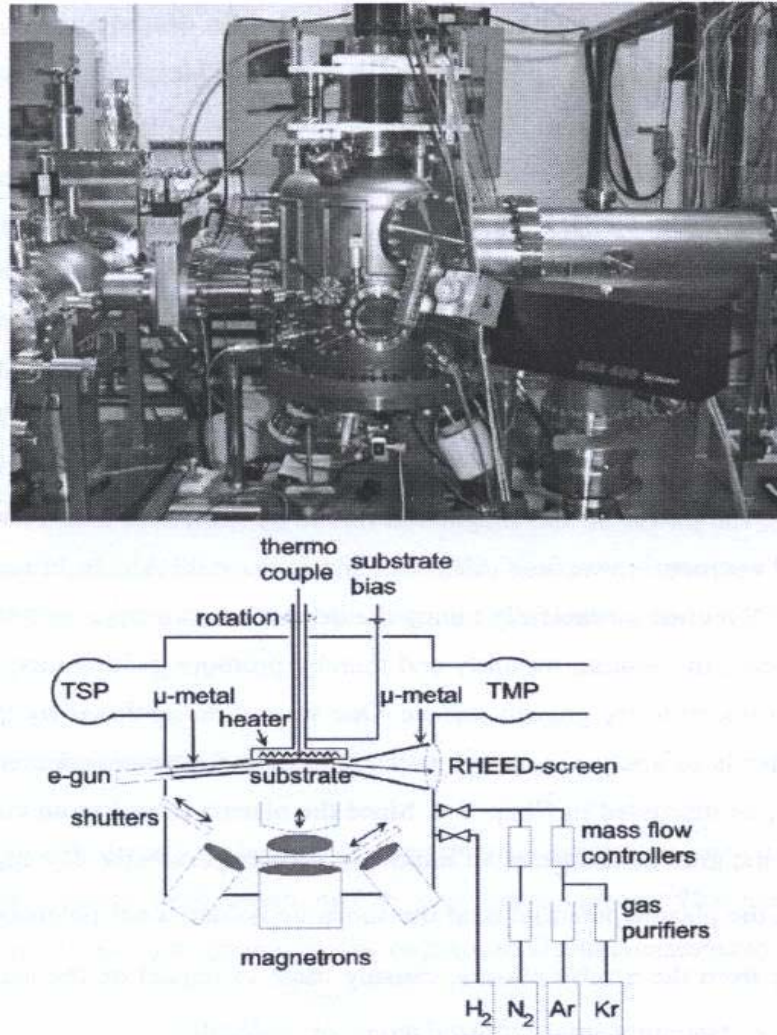


Fig. 2. The UHV system Ragnarök used in this project with a systematic overview showing the parts comprising the system [2.3].

2.2 Halide Vapour Phase Epitaxy (HVPE)

Considering the growth of gallium nitride, we can grow it by using several different techniques. The commonly used techniques are Molecular Beam Epitaxy (MBE), High Pressure Solution growth, Metallic Organic Chemical Vapour Deposition (MOCVD) and Halide Vapour Phase Epitaxy (HVPE) etc. Each of the above mentioned techniques are important for some specific applications but one of the most promising techniques for growing thick and large area layers is HVPE. HVPE is well known growth technique for growth of thick GaN layers of high crystalline quality due to its high growth rate and low cost. The growth rate ranging from about 30 micrometers up to few hundred micrometers per hour. By HVPE, we can easily achieve thick GaN layers up to several hundreds of micrometer. However, the maximum size of free standing GaN is still limited because of the cracking and fracture of thick GaN films [2.5]. The thick layer of GaN grown by HVPE can be used as native substrate for the growth of devices with other techniques. The first freestanding thick layer of GaN was obtained by HVPE by using a sputtered ZnO buffer layer on substrate where the substrate was peeled off by using tweezers [2.7].

The growth of GaN by HVPE is a complicated process. Many factors contribute to the resulting quality of the grown layers. In this growth technique (HVPE) parameters like reactor design, carrier gases and precursors are very important in order to obtain good quality GaN [2.8].

The growth of GaN by using HVPE growth technique has some advantages as well disadvantages. Advantages are, high growth rate, relatively low cost, and high crystal quality and disadvantages are, harsh environment, Si and O₂ impurities from quartz tube, long cleaning time between growth runs, and difficult to obtain p - type doping.

2.2.1 Chemistry

In conventional HVPE, ammonia is used as nitrogen source and GaCl as a Ga source. The GaN is formed in the growth zone as a result of a chemical reaction between Gallium chloride and ammonia at high temperature (1050°C). The chemical reaction in this whole process of growth takes place in two steps.

In first step GaCl_(g) is formed. To get this (GaCl_(g)), HCl gas is introduced in the zone where the boat containing Ga metal is placed as shown in fig. 3. Then a chemical reaction between Ga metal (liquid form) and HCl gas takes place at 850 °C in order to give GaCl_(g) according to reaction (1). The conversion efficiency to produce GaCl at 850 °C is found to be above 95% [2.4]. The chemical reaction-taking place in this zone is shown below in the form of a chemical equation.



In the second step, source gases (GaCl and NH₃) are introduced in the growth zone; GaN on the substrate is formed as a result of chemical reaction between ammonia and GaCl at growth temperature ranging from 1000 °C to 1100 °C. The chemical reaction takes place during the growth process of GaN is shown in the form of a chemical equation (2).



The overall chemical reaction-taking place inside the growth reactor (HVPE) can be written as in (3).



In HVPE, N₂ and H₂ are commonly used as carrier gases. During chemical reaction, NH₄Cl is formed in the form of fine white powder in large amount. It is very important to handle this white powder; otherwise it can block the exhaust pipes. To overcome this problem, traps are usually connected with reactors [2.7 and 2.8].

2.2.2 Reactor design

The reactor design is very important in the growth of high quality single crystalline GaN. As for the reactor geometry concerned, we can divide HVPE reactors in two groups

- Horizontal HVPE Reactor
- Vertical HVPE Reactor

Horizontal HVPE reactor is the most commonly used geometry. The schematic diagram of a horizontal hot wall reactor is shown in fig. 3. This reactor consists of a long quartz tube, which is heated from the walls by a multizone oven. This reactor is used to grow layers in the range of few micrometers to about 100 micrometers. This reactor is not suitable for the growth of thicker layers due to parasitic deposition that creates problems with changes of the growth conditions.

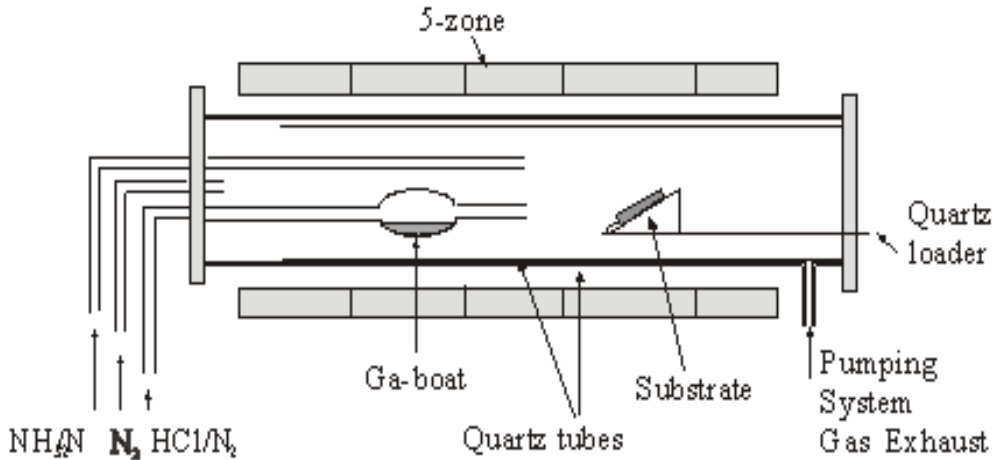


Fig.3. Schematic diagram of HVPE horizontal reactor design

A vertical HVPE reactor is an alternative geometry that we have used in our project. In this geometry, precursors can be introduced either from the top or from the bottom. If we introduce precursors from the top, we have to face one problem that particles of parasitic growth in the inlet can fall on the substrate and can cause defect nucleation centres and destroy the quality of grown crystals. This type of problems can be avoided by introducing the precursors from the bottom. The schematic diagram of a bottom feed HVPE reactor used in our project is shown in fig. 4. This reactor is designed to grow thick layers of GaN up to several millimetres. In order to keep a constant distance between surface of the sample and inlet. This reactor has the facility of pulling of the sample holder. In addition to this, the reactor has the facility of rotation of the sample holder in order to obtain uniform deposition of GaN.

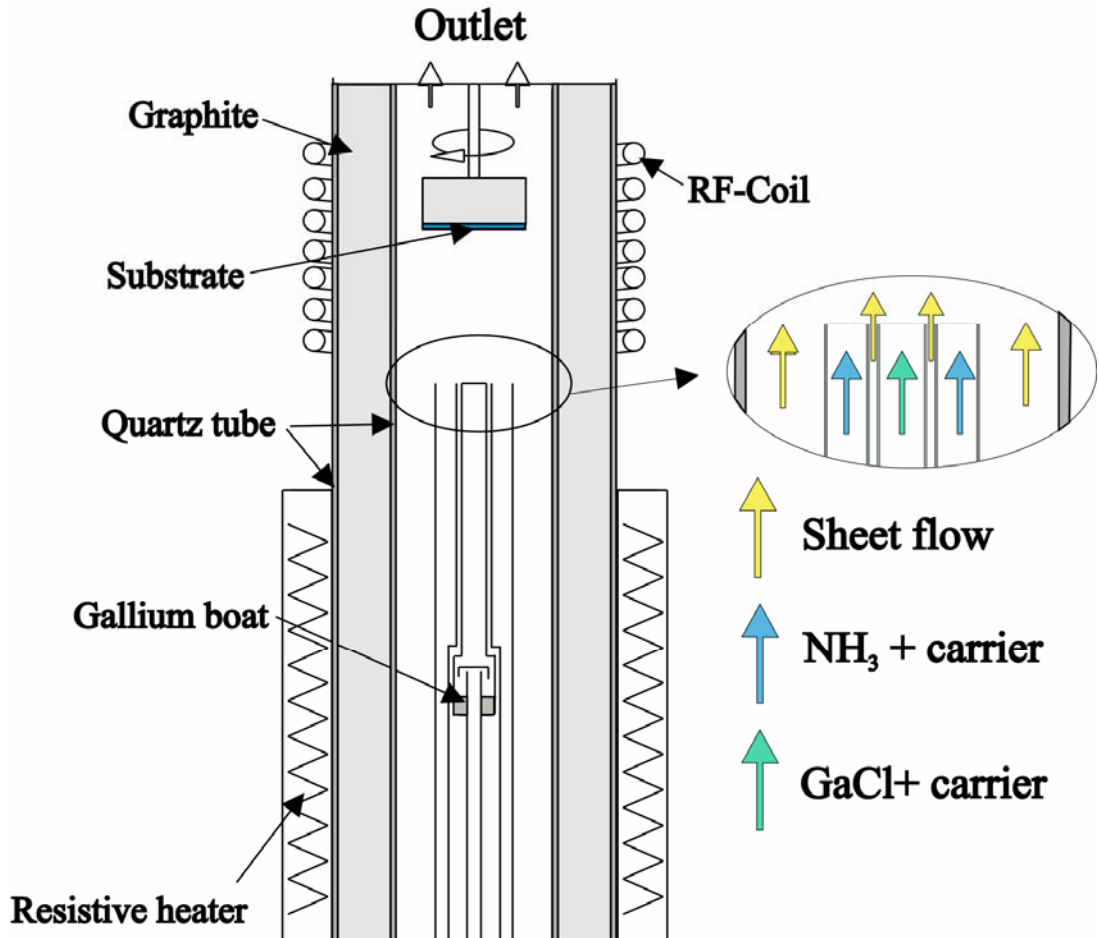


Fig.4. Schematic diagram of HVPE vertical reactor design.

In this hot wall HVPE reactor, a resistive heater heats the Ga boat-containing region to 850 °C and RF coil heats the growth region to about 1050 °C by induction. RF coil induction heating provides faster and precise control over the temperature in the growth zone. Parasitic deposition at the inlet of the reactor and on the walls of the reactor is a big problem in HVPE growth of thick GaN layers. In order to avoid parasitic deposition at the inlet of the reactor, the reactor is designed in such a way that premature reaction between NH₃ and GaCl can be avoided by sheet flows. In addition to the inlet sheet flows preventing GaCl to react with ammonia, a sheet flow near the walls of reactor can be seen in the insert of fig. 4 that prevents parasitic deposition on walls of the reactor.

In the HVPE process the conversion ratio of HCl to GaCl is very important because it affect the growth rate as well as etching component in the growth process. By careful designing of the Gallium boat, conversion efficiency up to 98 % can be achieved in a vertical reactor [2.9]. That is close to chemical equilibrium at 850 °C. [2.10]

In order to get desirable mass transport behaviour, we need to have a stable, vortex free flow field in the reactor. The circulation flows can give rise to non-uniform growth rate, less control on parasitic growth and increase of impurity incorporation. It has been shown that by minimizing the circular flow in the reactor, the run-to-run reproducibility is improved drastically [2.11].

Chapter 3: Characterization Techniques

3.1 X-Ray Diffraction (XRD)

X-rays are defined as electromagnetic radiation of exactly the same nature as light but of very much shorter wavelength. They were discovered by the German physicist Wilhelm Conrad Röntgen in 1895 who received the first Nobel prize in physics in 1901 for his discovery [3.1]. X-rays can be used in different scientific fields (chemical, physical, and medical fields, etc...). In the medical field as an example, they are used for images. Relatively low-energy X-rays can pass easily through the brain, and by increasing their energy they can pass through the soft tissues. It is also used to give information about the composition of the elements in a material, grain size, strain in the crystal lattice, thickness, surface roughness, residual stress, and texture (the preferred orientation of the grain in the material).

X-ray diffraction is one of the most important analytical techniques since it can yield a lot of information about the crystal. It can be used to identify the crystalline phases in the material by scanning over the unknown sample and compare the obtained diffraction pattern with an internationally recognized data base (JCPDS) which containing more than 70,000 phases [3.2].

3.1.1 X-Ray Generation

X-rays are produced when high speed electrically charged particles (electrons) generated from a filament are decelerated in a target. When they bombard it, most of their kinetic energy is converted into heat, and the rest is transformed into X-rays. This kind of radiation is called “bremsstrahlung” (breaking radiation in German). In addition to the bremsstrahlung, characteristic X-ray emissions will also occur from the target. Characteristic X-rays originate from electronic transitions between the core energy levels in the target atoms. The generated X-rays from Cu-target (Cu K α) have a wavelength of 1.5406 Å and can interact with the periodic crystal lattice in many ways. It can be reflected, absorbed, diffracted, or scattered [3.2]. Absorption involves the transformation of X-rays into kinetic energy of ejected electrons, where scattering is a process in which there is a transfer of radiation energy from the primary beam to scattered beams originating in the atoms of the absorber [3.3]. Schematic illustration of a modern x-ray tube is shown in Figure 3.1.

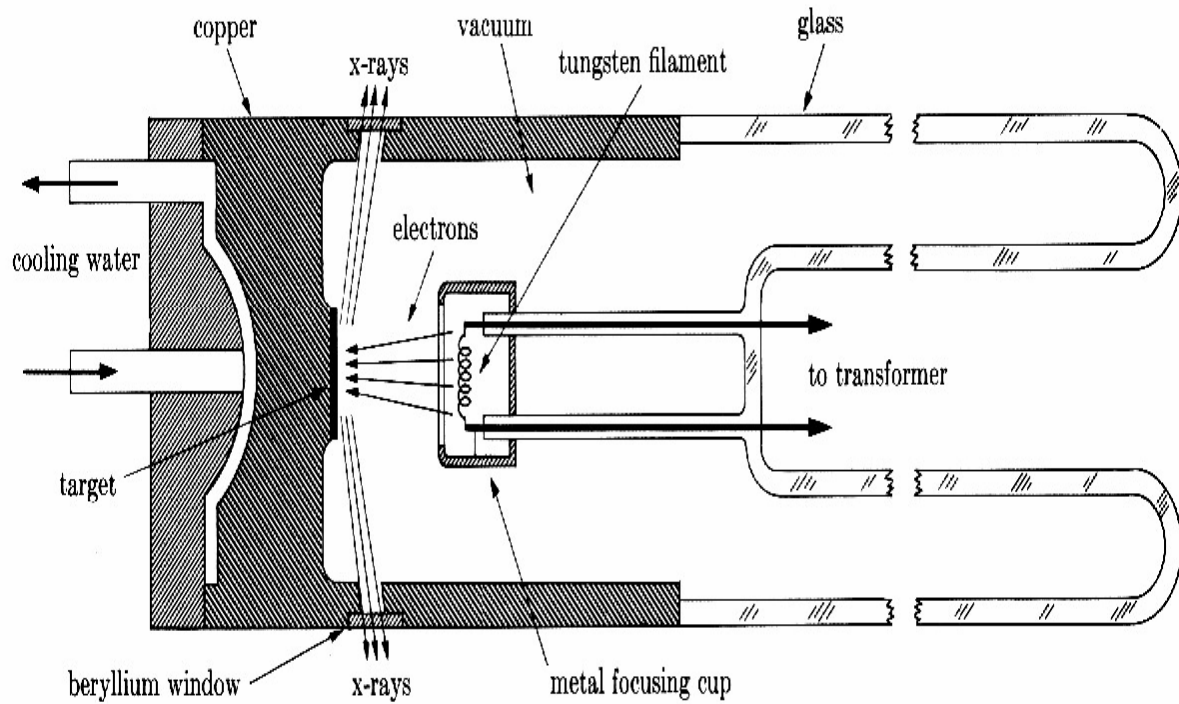


Fig 3.1 Schematic illustration of a modern x-ray tube [3.4].

3.1.2 Bragg's Law

The 3D crystal lattice is built up by atoms arranged in a regular and repeated pattern, the distribution of these atoms could be unlimited in space. The characteristic repetition distance of the atoms are noted by the lattice parameters a , b , and c in the three dimensions, and these atoms arrange themselves to form series of parallel planes.

In X-ray diffraction, the incident X-rays that hit the atoms which are arranged in different planes in a crystal, are scattered in all directions. Constructive interference require that the scattered beams come out in phase, which means that the path difference between the incident and outgoing rays equal an integral number of wave lengths, this is called Bragg's law, and explain the condition of the diffraction. The statement of Bragg's law is:

$$2d \cdot \sin \theta = n\lambda \quad (3.1)$$

Where d is the interplaner spacing, λ is the X-ray wavelength, and θ is the angle between the incident X-ray and the atomic planes. Figure 3.2 shows schematic Bragg reflection from the lattice planes.

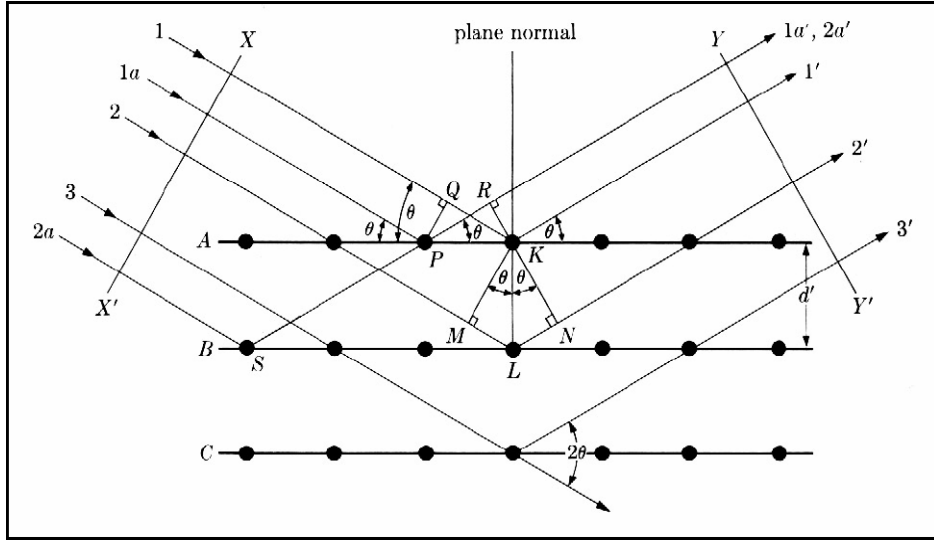


Fig.3.2. Schematic Bragg reflection from a set of lattice planes in a crystal. [3.4].

3.1.3 Reciprocal Space Mapping (RSM)

The crystal planes are defined by miller indices ($h k l$) which represent spacing and orientation of planes in the crystal coordinate system. Each set of planes in real space is related to a point in the so-called reciprocal space. The reciprocal lattice is the Fourier transformation of the charge distribution in the real lattice. However, a simplified construction of the reciprocal lattice can be made by plotting, in a coordinate system, for each set of lattice planes reciprocal lattice points along the direction of the plane normal a distances from the origin which are inversely proportional the plane spacing.

If an incident monochromatic wave is elastically scattered from the sample, both the incoming (k) and the scattered wave vector (k') will have the same magnitude, [3.5]

$$|k| = |k'| = \frac{2\pi}{\lambda} \quad (3.2)$$

The resulting reciprocal scattering vector (q) is equal to

$$|q| = |k - k'| = \frac{4\pi}{\lambda} \sin \theta \quad (3.3)$$

Where λ is the X-ray wavelength, θ the angle between the incident X-ray and the atomic plane, k is the incoming wave vector, and k' is the scattered wave vector. Whenever the scattering vector coincides with a reciprocal lattice points, diffraction will occur. This is equivalent to Bragg's law represented in

reciprocal space. It can be illustrated by the use of the so-called Ewald's sphere construction. Fig 3.3 shows Ewald sphere construction.

The shape of the reciprocal lattice points give information about the sample quality and is measured by the reciprocal space mapping (RSM). The full width at half maximum (FWHM) of the points in different directions depend on several factors such as stress, texture, dislocation, etc.

"Ewald sphere" is drawn with a radius equal to $|k| = \frac{2\pi}{\lambda}$. Its radius vector is set equal to the incident beam direction pointing at the origin of reciprocal space. Then, if the surface of the Ewald sphere gets in contact with a reciprocal lattice point, diffraction occurs.

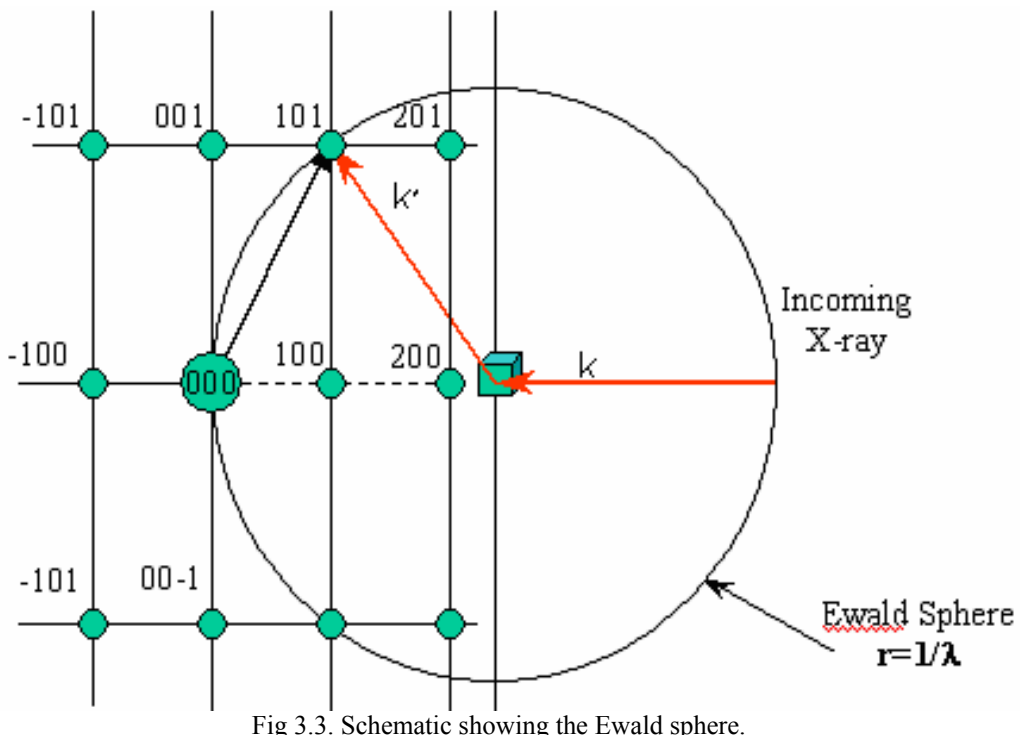


Fig 3.3. Schematic showing the Ewald sphere.

3.2 Transmission Electron Microscopy (TEM)

A transmission electron microscope (TEM) basically looks similar to an optical microscope, the only differences are that the optical microscope use photons to illuminate the sample instead of electrons, and glass lenses instead of magnetic lenses.

TEM is used to study the microstructure of semiconductors, alloys, and biological systems [3.6] and works by accelerating high energetic electrons to penetrate the sample. Materials for TEM must be specially prepared to thicknesses that will allow electrons to be transmitted through the sample and high vacuum is required to enable the electrons to reach the sample (long mean free path of the electrons).

A TEM system consists of the following components:

- Electron source at high negative potential surrounded by “Wehnelt cylinder” and an anode which forms a beam of electrons
- Two condenser lenses to focus the electron beam on the sample.
- Objective lens, which is a very important and critical component in the microscope since the resolution highly depends on it.
- Intermediate and projector lenses. Both of them are used for the image magnification.
- Objective aperture in the objective back focal plane to improve the contrast.

There are two different ways to create the image in TEM, phase contrast and diffraction contrast. In phase contrast, electrons leaving the TEM sample are recombined so that the phase differences from two or more beams are converted into intensity differences in the image, while in the diffraction contrast the diffracted electrons leaving the exit surface of a crystalline TEM sample are either collected for, or prevented from, contributing to an image [3.7]. Figure 3.4 shows a schematic of the TEM electron optics.

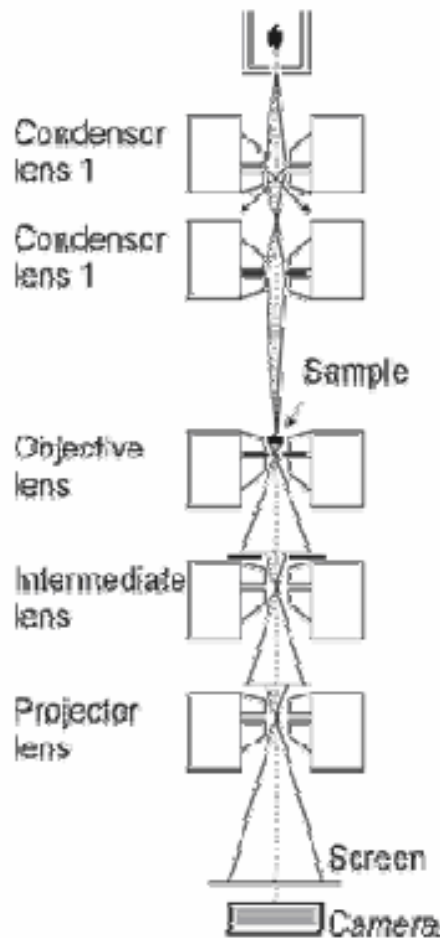


Fig 3.4. Schematic illustration of the lenses and apertures in a transmission electron microscope [3.6].

3.2.1 TEM sample preparation

For TEM measurements the sample must be prepared into a very thin foil, with a thickness of $\sim 50 \mu\text{m}$ to allow the transmission of the electrons.

In this work the samples were prepared for cross-sectional viewing by ion-beam thinning technique. First the samples were cut out to two small slices ($1\text{mm} \times 1.8\text{mm}$) and glued face to face in a titanium grid. The sample was then polished by using different polishing papers till it reached a thickness of $\sim 50 \mu\text{m}$. At the final step the samples were etched by Ar^+ ions in a rapid etching system BAL-TEC RES 101.

3.3 Cathodoluminescence (CL)

CL has high spatial resolution and it is used to study impurities and defects in semiconductor material. It gives information about the electronic band structure, and the distribution of defects. It can also give more detailed depth-resolved information by changing the electron beam energy.

The CL signal is formed when a highly focused electron beam bombards the sample causing the sample to emit photons from a localized area. These photons are emitted as a result of electronic transitions between the conduction and valance bands and levels lying in the band gap of the material [3.8]. The photons are collected with a detector and by scanning the electron beam on the sample, an image of the intensity over the sample is obtained.

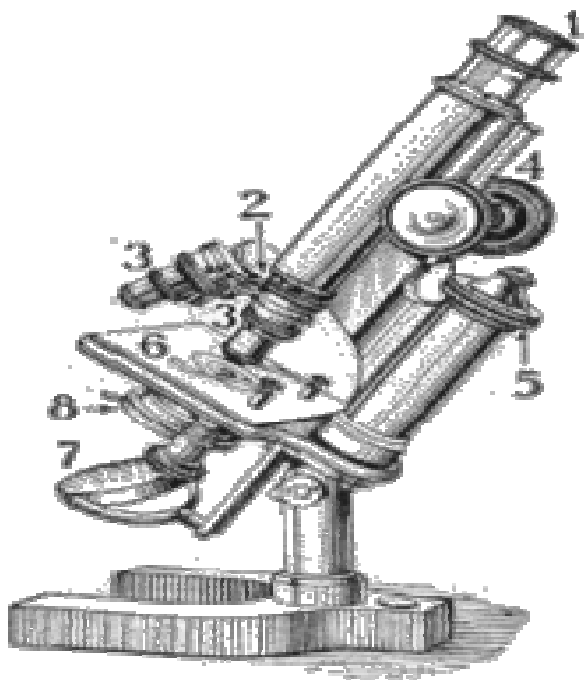
Cathodoluminescence is performed in a vacuum chamber and is attached to a TEM or a scanning electron microscope (SEM). In both of these cases the sample is excited by an electron beam on the sample.

The cathodoluminescence measurements were done in a MonoCL2 system from Oxford Instruments attached to a Leo 1550 FEG SEM system. In order to improve the resolution, the measurements were performed at liquid He temperature (4K). From this system it is possible to see SEM image, and by changing the detector it is possible to measure CL images in monochromatic and panchromatic mode. In monochromatic mode it is also possible to measure CL spectra.

3.4 Optical Microscope (OM)

A microscope is an instrument for viewing objects that are too small to be seen by the naked eye. The science of investigating small objects using such an instrument is called microscopy, and the term microscopic means very small, not easily visible with the naked eye (requiring a microscope to examine).

The optical microscope is the most common type of microscope, containing one or more lenses to magnify images of an object placed in the focal plane of the lens (es). In the optical microscope the light often pass through the specimen but can also be reflected off the surface into the objective lens. Fig [3.4] shows the main components of the optical microscope.



1. Ocular lens or eyepiece
2. Nosepiece with objectives
3. Objective lenses
4. Coarse adjustment knob
5. Fine adjustment knob
6. Object holder
7. Mirror
8. Diaphragm and condenser

Fig [3.4]. Shows the main components of the optical microscope:

Chapter 4: Experimental details and characterisation of Al_{1-x}In_xN seed layer

4.1 Sample preparation

4.1.1 Wafer cutting

In this project, we have been growing on 10mm×10mm samples and two-inch diameter samples. In order to prepare 10mm×10mm samples of sapphire, we had to cut two inch sapphire wafers. In order to minimize the risk of dropping the substrates inside the deposition system, the size of the substrate must be very accurate. The precise cutting of the sapphire wafer (substrate) was done in the wafer-cutting lab of Linköping University by using wafer-cutting machine “Cuto 1”.

Before loading the wafer on the wafer cutter “Cuto 1” the wafer was glued with wax on a wafer holding plate. The wafer holding plate was attached to a table that can move in the xy direction. The wafer cutting was done by a diamond blade. The speed of the diamond blade and the xy table was adjusted to 2200 rpm and 2.2 mm / minute respectively.

4.1.2 Cleaning process of samples

To remove contaminations from the wafer cutting process, the samples were cleaned. Contaminations like heavy residue and fingerprints etc were removed in the following way.

- Swabbing with Q-tip dipped in TCE (Tri Chloro Ethylene)
- Warming in TCE (Tri Chloro Ethylene) for five minutes
- Dipping in Acetone for three minutes
- Dipping in Ethanol for three minutes
- Rinsing with DI water.

The organic contaminations were removed by TL1 cleaning process in the following way.

- 5 parts water (H₂O)
- 1 part 25 % ammonia (NH₃)
- 1 part 30 % hydrogen peroxide (H₂O₂)

The samples were dipped and heated at 85 °C in a solution of water, ammonia and hydrogen peroxide prepared in the above-mentioned composition for five minutes. Finally the samples were rinsed in DI water. The process of rinsing with DI water was repeated ten times.

The inorganic contaminations and particles were removed by the TL-2 cleaning process in the following way.

6 parts water (H_2O)
 1 part 37 % hydrochloric acid (HCl)
 1 part 30 % hydrogen peroxide (H_2O_2)

The samples were dipped and heated at 85 °C in a solution of water, hydrochloric acid and hydrogen peroxide prepared in the above-mentioned composition for five minutes. Finally the samples were rinsed in DI water. The process of rinsing with DI water was repeated ten times [4.1].

The clean samples were dried with nitrogen and placed in cleaned sample boxes. Before transfer of these cleaned substrates to the UHV chamber of “Ragnarök”(Reactive Magnetron Sputtering system) for the growth of TiN buffer layer and AlInN seed layer, these substrates were cleaned in a three-step ultrasonic bath procedure. These steps consist of 5 minutes ultra sonic cleaning in trichloroethylene, acetone and iso-propanol respectively.

4.1.3 Cleaning process of sample holders

In order to remove any contamination that may influence the growth process, the substrate holder was cleaned before fixing the substrate on proper place on the substrate holder. The substrate holder was dipped in a solution of 4 % Deacon / Neutracone and placed in an ultrasonic bath for ten minutes. Finally the substrate holder was rinsed in DI water. The process of rinsing with DI water was repeated three times.

4.2 Magnetron Sputter Deposition of TiN buffer and AlInN seed layers

4.2.1 De-gassing of samples

Before the deposition of the TiN buffer layer and the AlInN seed layer, all substrates were de-gassed in order to reduce surface contaminations. The Sapphire substrates were de-gassed by heating up to 1000 °C for half an hour while MgO and Spinal substrates were de-gassed by heating up to 1000 °C for one hour.

4.2.2 Growth of TiN buffer layer

To grow the TiN buffer layer, the substrate was cooled down to growth temperature i.e. 640 °C. The deposition conditions for the TiN buffer layer are given in table.1.

Table.1. Growth conditions for the TiN buffer layer.

Base Pressure	1.8×10^{-8} Torr	Deposition Time	8:30 Minutes
Thickness	500 Å	Deposition Rate	1 Å / Sec
Rotation	60 rpm	Argon Pressure	4.01 mTorr
Substrate Temp. (Ts)	640 °C	Nitrogen Pressure	0.31 mTorr
Substrate Bias (Vs)	-30 Volts	Total Pressure	4.32 mTorr
B.G Pressure at (Ts)	2.2×10^{-8} Torr	Power on Ti Target	350 Watt

Under these deposition conditions, the TiN buffer layer was deposited in UHV dc reactive magnetron sputtering chamber by using 99.999 % pure three-inch disc shaped elemental target of Ti metal. The target was positioned 30° off of the substrate normal. The target to substrate distance was 15 cm. During the deposition the substrate was rotated in order to get uniform deposition. The Ti target was sputtered by using 99.999999 % pure nitrogen gas diluted with 99.999999 % pure argon at a pressure of 4.32 mTorr. The Ti target was sputter cleaned for five minutes prior to deposition. The TiN film thickness was measured by X-rays reflectivity in order to determine the growth rate under these growth conditions. The calculated growth rate was nearly 1.03 Å / sec. The X-ray reflectivity scan is shown in Fig.1.

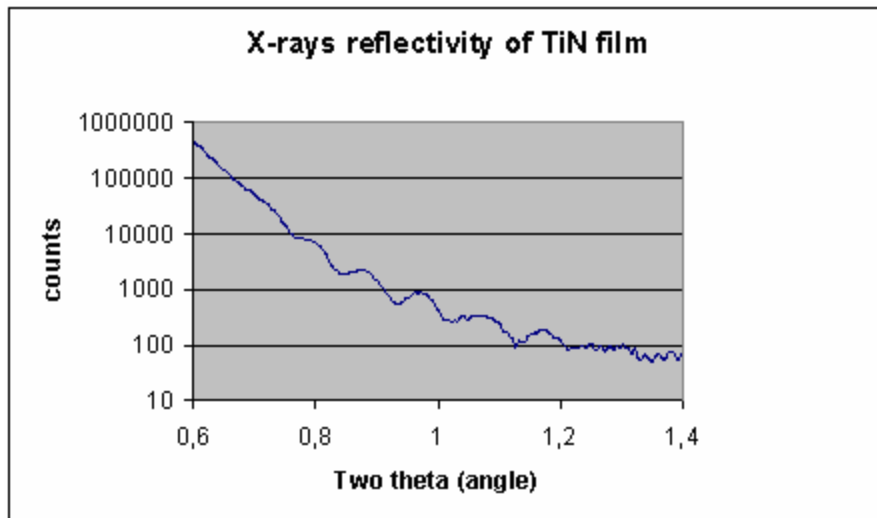


Fig.1. X-Rays reflectivity's scan of TiN buffer layer.

The TiN buffer layer provides less lattice mismatch as well as serve as an absorption layer and thus enabling an accurate temperature control of the substrate. The physical appearance of TiN plasma under deposition conditions given in table.1 is shown in fig.2.

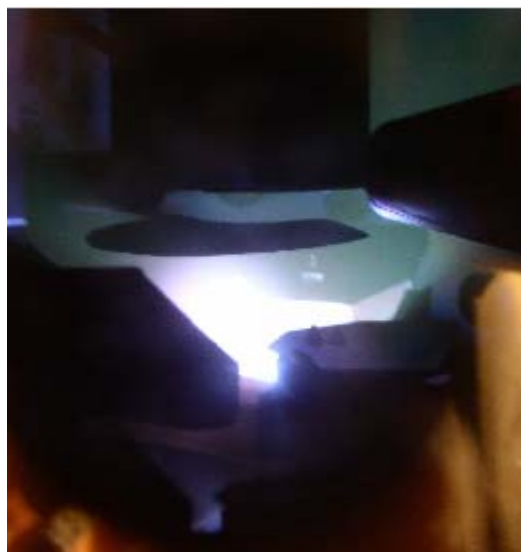


Fig.2. Physical appearance of TiN plasma.

4.2.3 Growth of $\text{Al}_{1-x}\text{In}_x\text{N}$ seed layer

After the growth of the TiN buffer layer, the samples were cooled down to the growth temperature of $\text{Al}_{1-x}\text{In}_x\text{N}$ at 230 °C. The $\text{Al}_{1-x}\text{In}_x\text{N}$ layer were deposited on top of the TiN buffer layer by using a 99.999 % pure three-inch elemental Al target and a 99.999 % pure two inch elemental In target. The $\text{Al}_{1-x}\text{In}_x\text{N}$ alloy films were grown by simultaneous co-sputtering from both the targets (Al & In) by using 99.999999 % pure nitrogen as a sputtering gas at a pressure of 10 mTorr. Both targets were positioned 30° off of the substrate normal opposite to each other and pointed at a common focal point where the substrate was located. The target to substrate distance was 15 cm. The substrate was rotated at a speed of 60 rpm in order to get a uniform growth on the substrate. The targets were sputter cleaned for five minutes prior to deposition of the $\text{Al}_{1-x}\text{In}_x\text{N}$ alloy film.

In order to obtain a GaN lattice matched seed layer of $\text{Al}_{1-x}\text{In}_x\text{N}$, an optimisation procedure of the composition was done. The composition of $\text{Al}_{1-x}\text{In}_x\text{N}$ was controlled by varying the power on the aluminium magnetron and keeping the power on the indium magnet constant at 10 watt. In order to determine the composition, XRD measurements were done after each run. From these measurements, the required magnetron power settings were determined. The tested powers on the aluminium magnetron was in the range 200---420 watts in order to achieve the required result. The XRD diffractograms that were measured during the composition tuning are shown in Fig.3.

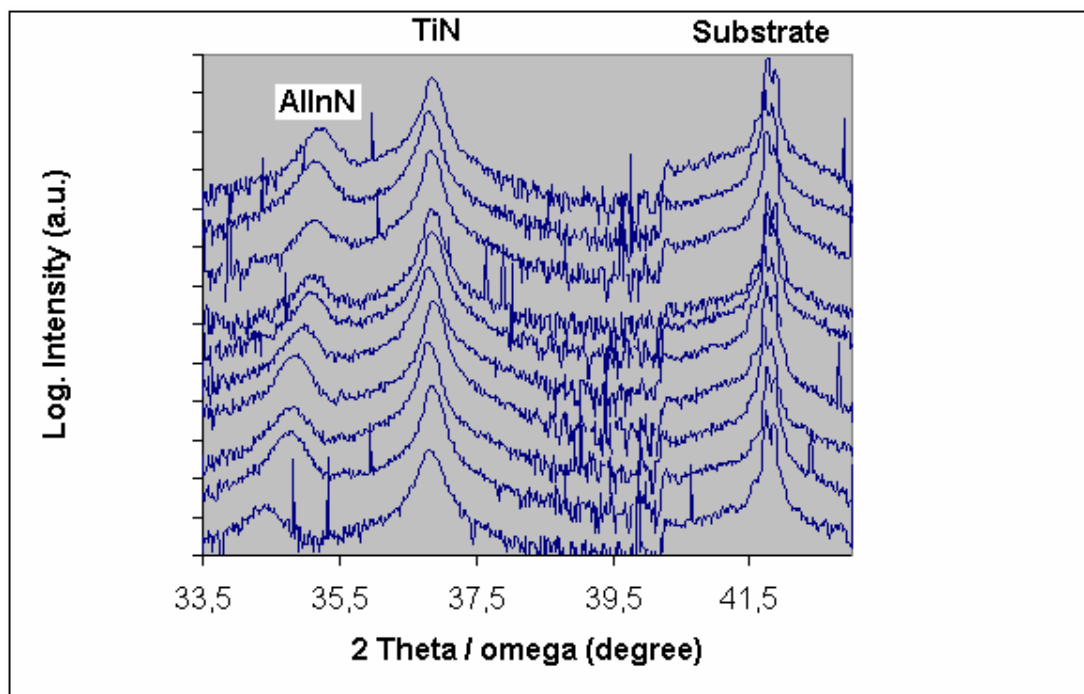


Fig.3. Compiled 2Theta / omega X-rays diffractograms of $\text{Al}_{1-x}\text{In}_x\text{N}$ film deposition. The $\text{Al}_{1-x}\text{In}_x\text{N}$ (0002) peak can be seen shifting left to right while going from bottom to top showing a variation in the indium composition ranging from $x = 31.5$ to $x = 16.25$ respectively.

The GaN lattice matched ternary alloy ($\text{Al}_{0.81}\text{In}_{0.19}\text{N}$) was achieved by applying a power of 340 watts on the aluminium magnetron. The growth conditions for the lattice matched ternary alloy ($\text{Al}_{81}\text{In}_{19}\text{N}$) seed layer are shown in table.2.

Table.2. Growth condition for ($\text{Al}_{0.81}\text{In}_{0.19}\text{N}$) seed layer.

Base Pressure	1.4×10^{-8} Torr	Substrate Bias	-30 Volts
B.G. Pressure at (Ts)	0.03 mTorr	Deposition Rate	1.02 \AA / sec
Nitrogen Pressure	10 mTorr	Power On Al target	340 Watt
Substrate Tem. (Ts)	230 °C	Power On In target	10 Watt

Different thicknesses of ($\text{Al}_{0.81}\text{In}_{0.19}\text{N}$) seed layer i.e. 250 Å, 500 Å, 1000 Å and 2000 Å were decided to be grown on sapphire, MgO and spinel substrates for the growth of GaN on top by Halide Vapour Phase Epitaxy. In order to control the thickness of the layers, growth rate was determined. The growth rate of $\text{Al}_{0.81}\text{In}_{0.19}\text{N}$ seed layer under deposition conditions given in table. 2 was determined by X-rays reflectivity. The X-rays reflectivity scan is shown in Fig. 4.

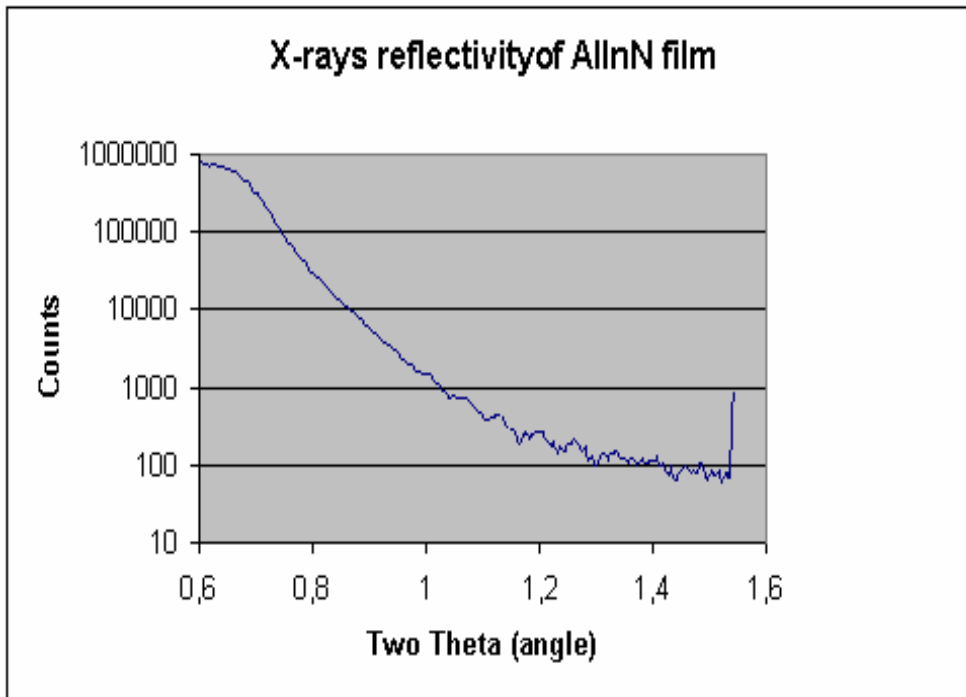


Fig.4. X-Rays reflectivity's scan of AlInN seed layer.

The growth rate that was calculated from x-rays reflectivity of $\text{Al}_{0.81}\text{In}_{0.19}\text{N}$ seed layer was 1.02 \AA / sec . From the calculated growth rate, different thicknesses of $\text{Al}_{0.81}\text{In}_{0.19}\text{N}$ seed layer i.e. 250 Å, 500 Å, 1000 Å and 2000 Å were grown on two inch diameter sapphire and 10mm×10mm MgO and spinel substrates.

$\text{Al}_{0.81}\text{In}_{0.19}\text{N}$ seed layer of different thicknesses i.e. 250 Å, 500 Å, 1000 Å and 2000 Å were characterised before growth of GaN on top by HVPE. Fig. 5 shows asymmetric (1 1 0) $2\theta - \omega$ XRD scans representing $\text{Al}_{0.81}\text{In}_{0.19}\text{N}$ seed layers of different thickness grown on two-inch diameter sapphire substrate. $\text{Al}_{0.81}\text{In}_{0.19}\text{N}$ seed layers of different thickness grown on 10mm×10mm MgO and spinel substrates also shows similar results. The in-plane lattice parameter “a” was calculated from (1 1 0) peak position

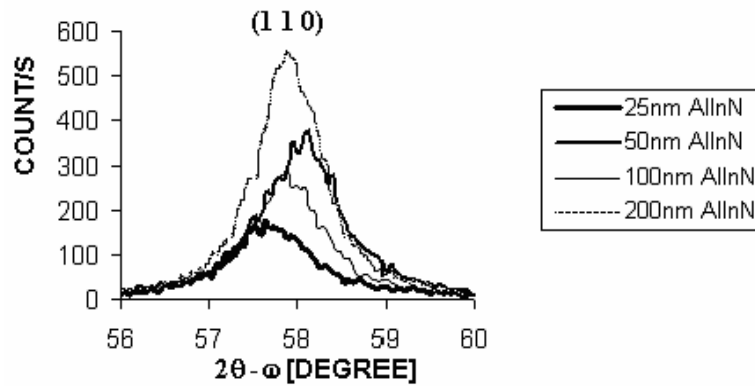


Fig. 5. $2\theta - \omega$ XRD scans representing 25 nm, 50 nm, 100 nm and 200 nm thick $\text{Al}_{0.81}\text{In}_{0.19}\text{N}$ seed layer.

In-plane lattice mis-match (Lattice parameter “a” mismatch) with the GaN in percentage was calculated by using the standard value of $a = 3.19\text{\AA}$ for GaN. The calculated results are shown in table. 3. A small difference in in-plane lattice parameter “a” can be seen in left column of this table.

Table. 3. Lattice parameter “a” and %lattice mismatch with GaN for different thickness of $\text{Al}_{1-x}\text{In}_x\text{N}$ seed layer.

Sample	Thickness (\AA)	$a(\text{Al}_{1-x}\text{In}_x\text{N})$ (\AA)	$a(\text{GaN})$ (\AA)	Lattice Parameter “a” Mismatch with GaN (%)
C	250	3.1916	3.19	0.05
D	500	3.1750	3.19	0.47
E	1000	3.1860	3.19	0.12
B	2000	3.1836	3.19	0.20

Physical appearance of AlInN plasma under deposition conditions given in table 2 is shown in Fig.6.



Fig.6. Physical appearance of AlInN plasma.

4.2.4 Summary of grown samples during composition tuning

The lattice parameter “c” was calculated from the 2θ (0002) peak. The indium composition “x” and the lattice parameter “a” was calculated by using vegards law given in equation (A).

$$C_{AlInN} = X C_{InN} + (1-X) C_{AlN} \quad (A)$$

To calculate the “a” and “c” plane lattice mismatch with GaN, the standard values for GaN ($a = 3.19\text{\AA}$ & $c = 5.19\text{\AA}$) were used. The indium composition was determined by RBS as well for some samples. The difference in indium composition can be seen from XRD and RBS because vegards law does not hold good for this (AlInN) ternary alloy [4.2]. The result summery is given in table.4.

Table. 4. summary of results obtained during composition tuning.

Sr.Number	2θ (0002) peak Position	XRD %Indium Composition	RBS % Indium Composition	Lattice Parameter (a) \AA	Lattice Parameter (c) \AA	Power on Al target (w)	Power on In target (w)	(a) Parameter Mismatch with GaN (%)	(c) Parameter Mismatch with GaN (%)
1	34.840	23	X	3.210	5.144	250	10	-0.626	+ 0.886
2	34.420	31.5	X	3.240	5.204	200	10	-1.567	- 0.270
3	34.755	25	22.6	3.215	5.156	270	10	-0.784	+ 0.655
4	34.796	24	X	3.211	5.140	300	10	-0.658	+ 0.963
5	35.107	17.76	X	3.181	5.106	420	10	+0.282	+ 1.618
6	34.956	20	17.4	3.194	5.128	390	10	-0.125	+ 1.195
7	35.154	16.84	X	3.177	5.100	380	10	+0.408	+ 1.734
8	35.184	16.25	X	3.177	5.096	400	10	+0.408	+ 1.811
9	35.137	17.64	16	3.184	5.110	370	10	+0.188	+ 1.541
10	35.076	19.32	18	3.191	5.120	340	10	+0.04	+ 1.349

4.3 HVPE Growth of thick layer of GaN

The thick layer of GaN was grown by HVPE on top of the lattice matched $Al_{0.81}In_{0.19}N$ seed layers grown on two-inch sapphire wafer and pieces of 10 mm \times 10 mm spinel and MgO substrates according

to the deposition conditions described in table. 2. The selected thickness of the $\text{Al}_{0.81}\text{In}_{0.19}\text{N}$ seed layer was 250Å, 500 Å, 1000Å and 2000Å. The $\text{Al}_{0.81}\text{In}_{0.19}\text{N}$ seed layers were characterised by XRD in order to determine in plane lattice parameter (a), out of plane lattice parameter (c) and the film stress before deposition of GaN.

Before loading the sample in the HVPE reactor, the samples were cleaned in order to remove fingerprints, heavy residue and solvents by

- ❖ Swabbing with Q-tip dipped in TCE (Tri Chloro Ethylene)
- ❖ Warming in TCE (Tri Chloro Ethylene) for five minutes
- ❖ Dipping in Acetone for three minutes
- ❖ Dipping in Ethanol for three minutes
- ❖ Rinsing with DI water.

The samples were dried with nitrogen and loaded in the HVPE reactor. The samples were heated up to growth temperature 1040 °C. During the heating, the samples were kept in a nitrogen atmosphere up to growth temperature. To study the effect of carrier gas on quality of GaN, the samples were grown with a mixture of nitrogen and hydrogen and in nitrogen only. The carrier gas flows and precursor gas flows were controlled by a computer. The growth rate of GaN under growth conditions given in table. 5 were estimated by measuring the weight of the sample before and after the growth. In both cases growth rate was 1.2 μm / minute. The substrate holder was rotated during growth in order to get a uniform growth on the sample. Table. 5 show growth conditions for the growth of GaN while using a mixture ($\text{N}_2 + \text{H}_2$) and only N_2 as carrier gas.

Table.5. Growth conditions for GaN while using mixture ($\text{N}_2 + \text{H}_2$) and only N_2 as carrier gas

Process parameters	Carrier gasses	
	N_2	Mixture ($\text{N}_2 + \text{H}_2$)
Carrier gas ratio	X	12 : 1
NH_3 flow rate	1000 ml / minute	1000 ml / minute
HCl flow rate	40 ml / minute	40 ml / minute
V/III precursor ratio	25	25
Cell pressure	1016 mbar	1007 mbar
Growth rate	1.2 μm / minute	1.2 μm / minute
Growth temperature	1040 °C	1040 °C
Ga boat temperature	850 °C	850 °C

Chapter 5: Results and Discussions

The GaN lattice matched $\text{Al}_{0.81}\text{In}_{0.19}\text{N}$ seed layer was grown on sapphire, MgO and spinel substrates. After the growth of GaN on the $\text{AlInN} / \text{MgO}$ substrate, it was found that the MgO substrate was very fragile. The morphology was also very bad. This could be due to decomposition of MgO layer that may contaminate the film with Mg which is a p-type dopant in GaN. Thus, the idea of using MgO as substrate was dropped.

The GaN was also grown on GaN lattice matched $\text{Al}_{0.81}\text{In}_{0.19}\text{N}$ seed layers grown on spinel substrate that gave more or less similar results to sapphire substrates. Due to unavailability of two-inch wafer of spinel substrate and high cost, the study was concentrated on sapphire substrates that are available in two inch sized wafer and very cheap as compared to spinel.

Four different thicknesses, 25 nm, 50 nm, 100 nm and 200 nm of $\text{Al}_{0.81}\text{In}_{0.19}\text{N}$ seed layers were decided to be grown on two inch sized sapphire substrates.

To study the effect of carrier gasses on crystalline quality of GaN, growth of the GaN in the HVPE reactor was carried out at atmospheric pressure by using a mixture of ($\text{N}_2 + \text{H}_2$) and only N_2 as a carrier gas. So on the basis of carrier gases, grown samples can be divided in to two categories.

Category I: (Growth of GaN by using a mixture of N_2 and H_2 as carrier gas)

Sample A = HVPE growth of GaN on top of 100 nm thick $\text{Al}_{0.81}\text{In}_{0.19}\text{N}$ seed layer
Sample B = HVPE growth of GaN on top of 200 nm thick $\text{Al}_{0.81}\text{In}_{0.19}\text{N}$ seed layer

Category II: (Growth of GaN by using only N_2 as carrier gas)

Sample C = HVPE growth of GaN on top of 25 nm thick $\text{Al}_{0.81}\text{In}_{0.19}\text{N}$ seed layer
Sample D = HVPE growth of GaN on top of 50 nm thick $\text{Al}_{0.81}\text{In}_{0.19}\text{N}$ seed layer
Sample E = HVPE growth of GaN on top of 100 nm thick $\text{Al}_{0.81}\text{In}_{0.19}\text{N}$ seed layer

MOCVD grown seed layer about 100 nm with 30 μm thick HVPE GaN on two inch sapphire substrate was selected for comparison. The reference sample was named as sample F.

The GaN lattice matched $\text{Al}_{0.81}\text{In}_{0.19}\text{N}$ (0002) epilayer thin films deposited at low temperature by reactive DC magnetron sputter deposition was reported to be stable up to 1100 °C in vacuum [5.1]. In order to check the thermal stability of the GaN lattice matched $\text{Al}_{0.81}\text{In}_{0.19}\text{N}$ (0002) epilayer thin films, a sample was heated and cooled in the same atmosphere (N_2) as we use before HVPE growth. The optical microscope picture of the sample was taken before loading in HVPE reactor and after heating and cooling. No visual changes can be observed in OM images. The optical images are shown in fig. 1.

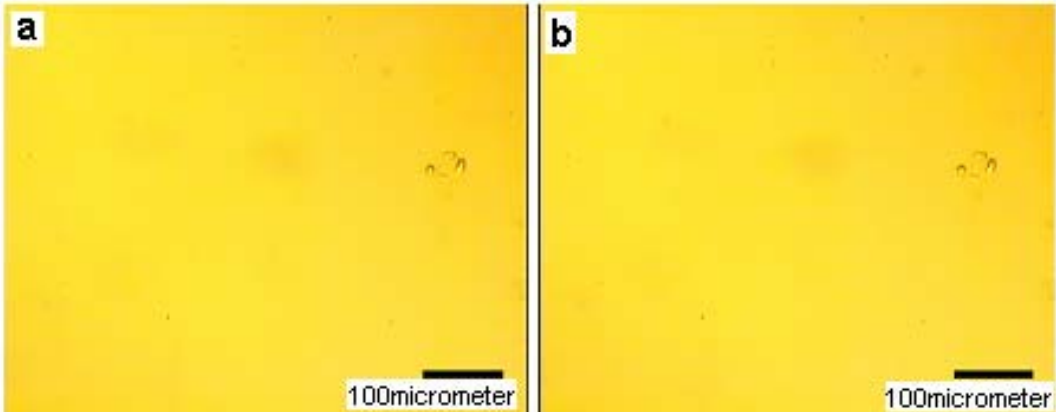


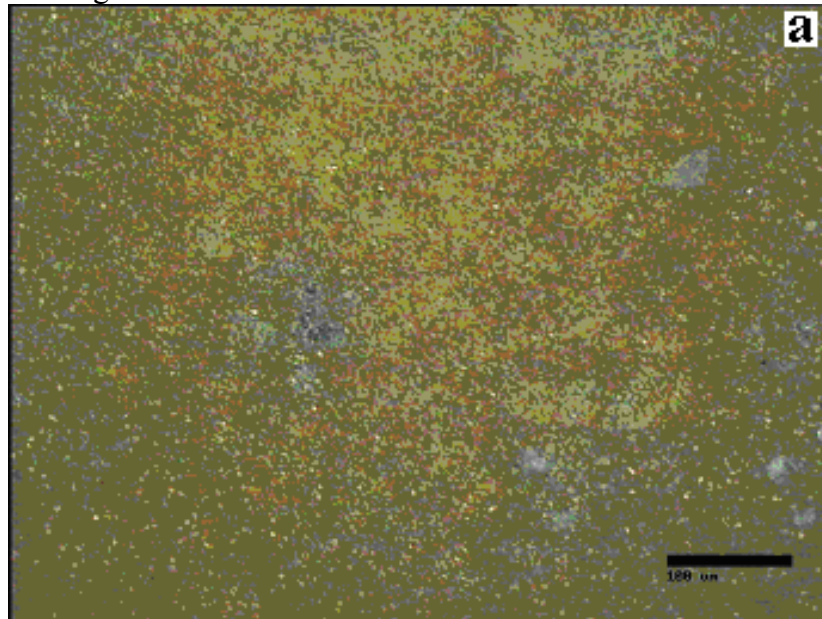
Fig. 1. Optical microscope picture of 50nm thick GaN lattice matched AlInN seed layer (a) Before loading to HVPE reactor (b) After heating and cooling.

5.1 Optical Microscope (OM) results

The images of the GaN surface were taken by optical microscopy (OM) to observe the surface morphology of the HVPE grown GaN. On the basis of used carrier gasses, OM measurements were divided in to two parts.

5.1.1 OM measurements on the samples grown by using a mixture of N₂ and H₂ as a carrier gas

The samples were grown on 2 inch sapphire substrate with the thickness of 100nm and 200nm seed layer. The thickness of the sapphire wafer was 360 μm . The optical microscope's micrographs that were taken are shown in Fig. 2.



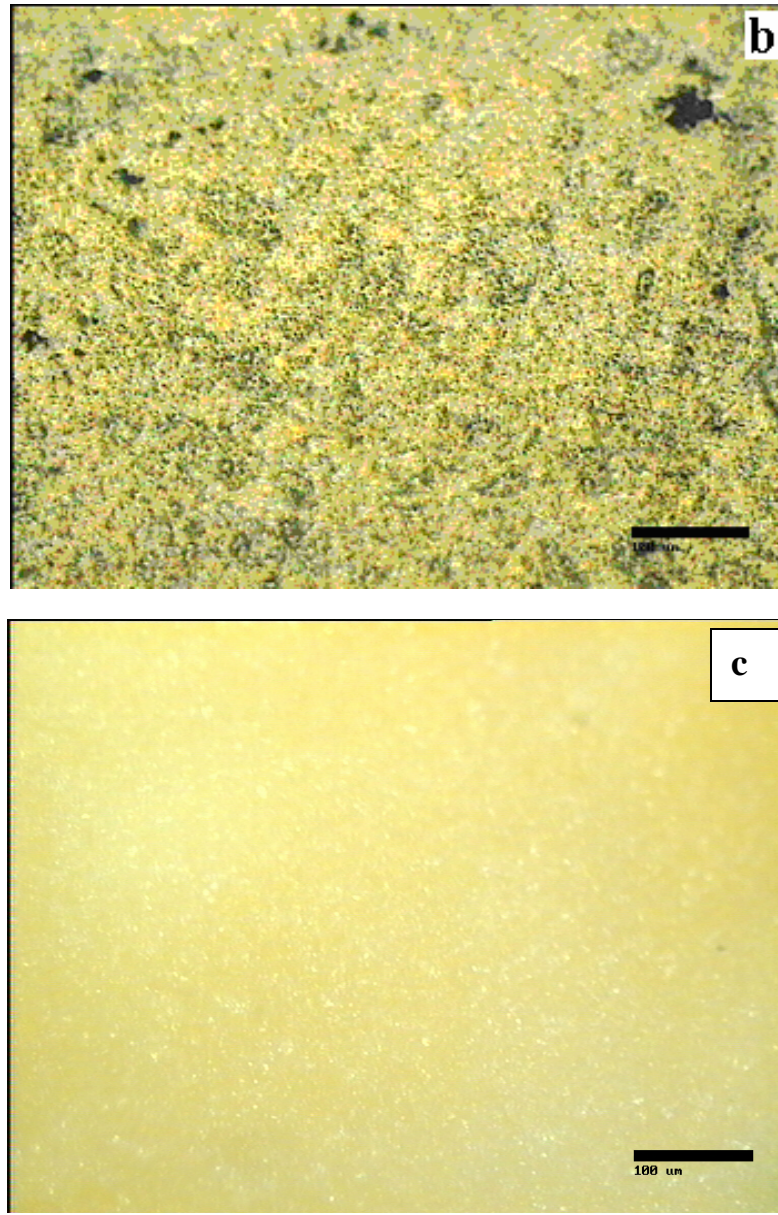


Fig. 2. OM images of GaN surface grown on AlInN seed layer by using a mixture of N₂ and H₂ as carrier gas (a) sample A, (b) sample B and (c) sample F.

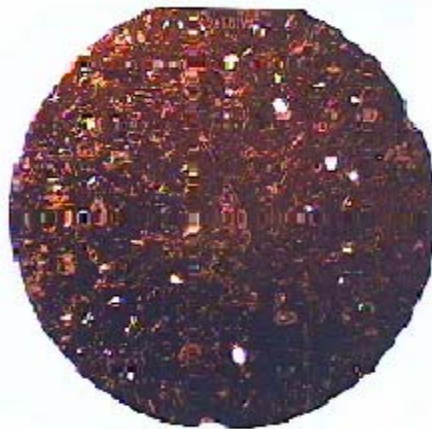
The OM images of the surface of samples A and B were taken after the growth of GaN by using mixture of H₂ and N₂ as a carrier gas during the growth. The surface morphology looks very bad and the quality of the GaN is very poor comparing with the reference sample F. Thus, the AlInN is very unstable in a hydrogen atmosphere so the growth of the GaN was continued by using only N₂ as a carrier gas.

5.1.2 OM measurements on the samples grown by using only N₂ as carrier gas

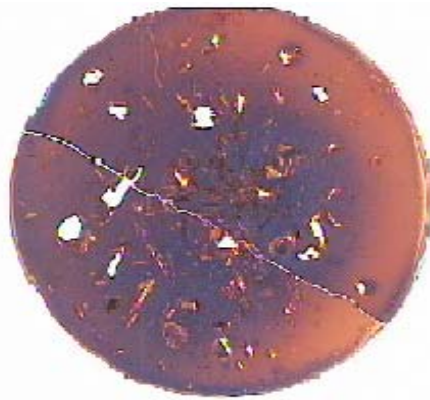
Optical microscope images of the full wafers of the samples that used only N₂ during the growth of GaN are shown in Fig. 3.



sample(c)



sample (D)



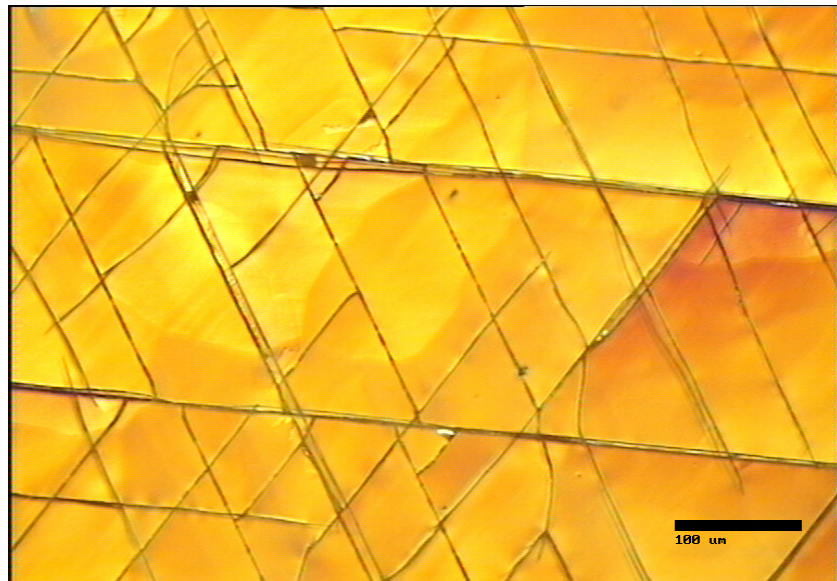
sample (E)

Fig. 3. Cracking of sapphire substrate and pealing off of GaN layer in small areas of samples (C, D, E).

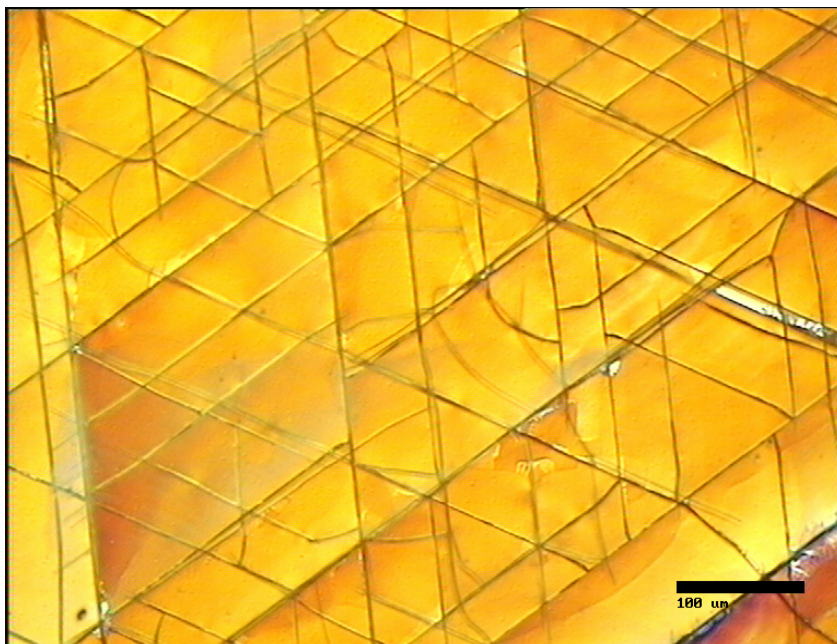
The sapphire substrates were cracked to many pieces, these cracks occur during and after cooling due to the compressive stress in the GaN. The reference sample doesn't show any cracks on the substrate, but the substrates of the other samples were cracked after cooling to small pieces. Separation

of small areas of GaN layers from the substrates for samples C, D, and E can be seen in Fig. 3. Where cracks intersect both each other and the film surface, the film has a tendency to lift away from the sapphire [5.2].

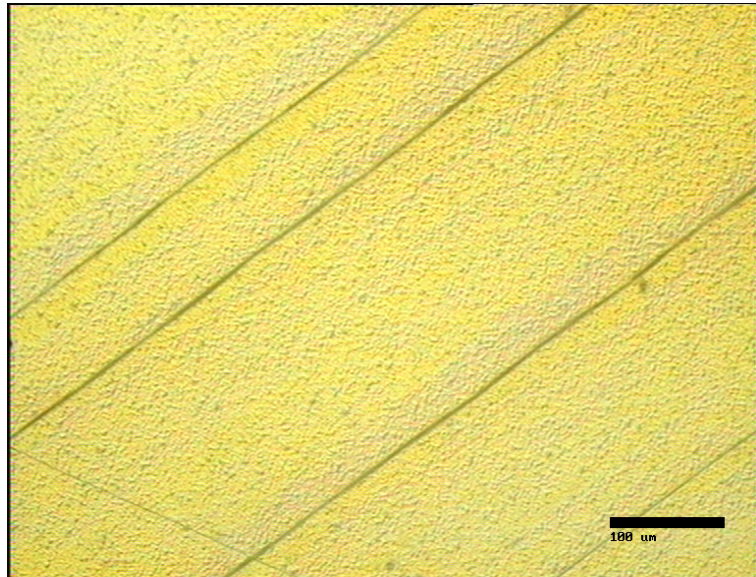
An OM images of small areas of the samples C, D, E, and F were taken with magnification 20x to get an over view of the surface of the GaN. The images are shown in Fig. 4.



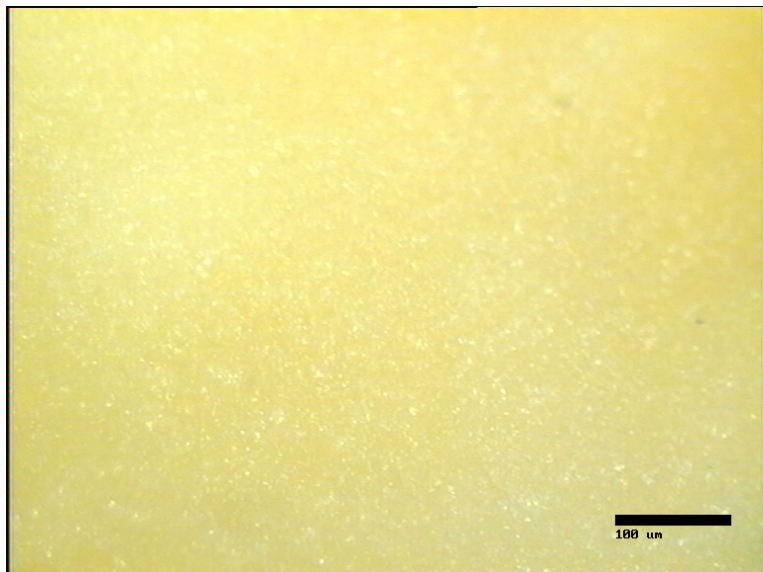
Sample (C)



Sample (D)



Sample (E)



Sample (F)

Fig. 4. OM images of GaN surface grown on AlInN seed layer by using only N₂ as carrier gas for samples C, D, E, and F.

The images show formation of cracks in the GaN films. These cracks occur due to the tensile stress during growth and it starts usually when the thickness of the GaN overcome some critical thickness. Cracking can be avoided if the film thickness is less than the critical value [5.2]. The critical value can be calculated by using the formula shown in mathematical equation (1).

$$h_{crit} = \frac{\Gamma_f \bar{E}_f}{Z \sigma_f^2} \quad (1)$$

Where Γ_f is the fracture toughness of the film, \bar{E}_f is the plane strain elastic modulus of the film, σ_f is the (uniform) film stress, and Z is the geometric factor that describes the crack shape.

The heating causes the lattice parameters to change and the difference in strain between substrate and grown GaN material can change in sign during heating or cooling [5.3]. GaN shows tensile strain at the growth temperature, but compressive strain at room temperature, this indicate that the GaN is under biaxial compressive stress due to the difference in thermal expansion coefficient and the difference in the lattice parameters between the GaN and sapphire.

Table. 1 lattice parameters and coefficients of thermal expansion for the sapphire and the GaN.

Material	Lattice parameters (\AA)	Thermal expansion coefficient ($10^{-6}/\text{K}$)
Sapphire	a= 4.758 c= 12.991	a= 8.11 c= 7.28
GaN	a= 3.19 c= 5.19	a= 5.59 c= 3.17

The concentration of the cracks varies between the samples, and is correlated with the thickness of the seed layer. It is clear that sample E with a thick seed layer (100nm) has fewer cracks comparing with the other two samples C and D (25nm and 50nm).

5.2 High Resolution X-ray Diffraction results

To understand the structural properties of the HVPE grown GaN, XRD measurements were performed. The XRD measurements were obtained by using Cu K- alpha radiations. The X-rays radiations source was operated at 40 kV and 40 mA. On the basis of characterized material, XRD measurements can be divided into two main parts.

1. Characterization of HVPE grown GaN using a mixture of N₂ and H₂ as a carrier gas.
2. Characterization of HVPE grown GaN using only N₂ as a carrier gas.

5.2.1 XRD measurements on samples grown by using mixture of H₂ and N₂ as carrier gas

The XRD measurements were done for the samples that grown by using mixture of H₂ and N₂ to determine the lattice parameters, the stress, and to investigate the quality of the GaN. The omega scans and 2 theta\omega scans for the 105 and 002 reflections are shown in Fig. 5.

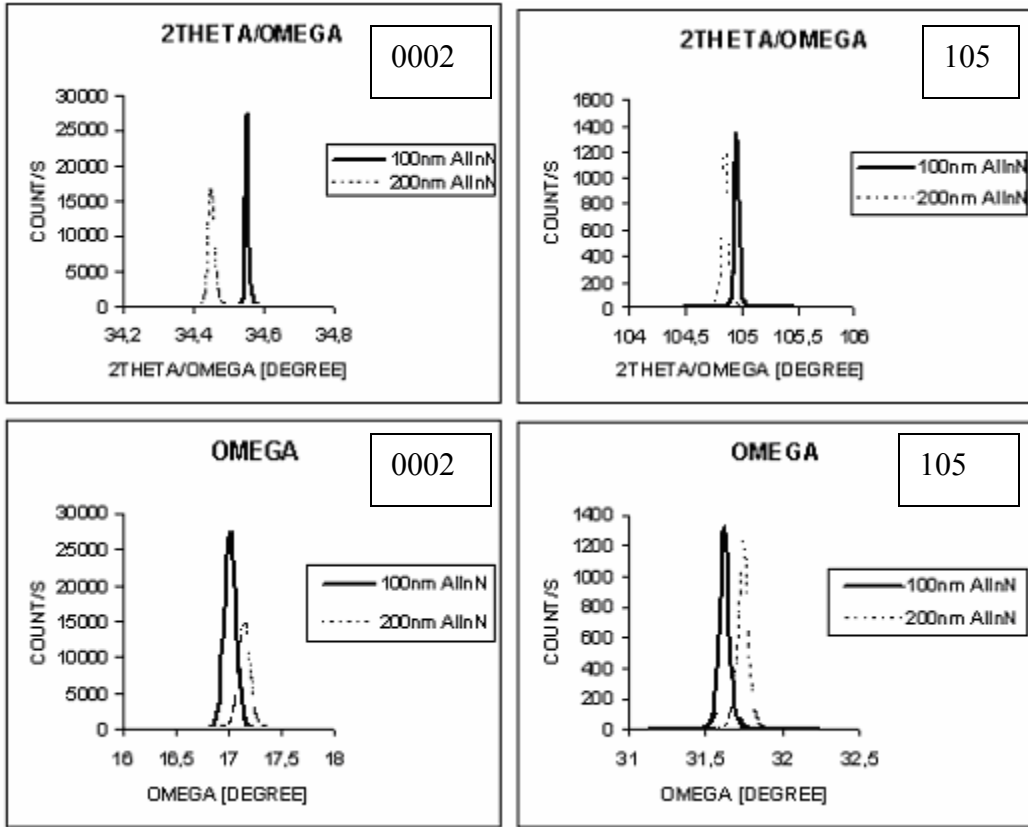


Fig. 5 the scans for the GaN samples grown by using mixture of H₂ and N₂.

The crystal quality of the thick GaN was estimated by HRXDR rocking curves measurements. The full width at half maximum values of the ω -scan from the 002 and 105 reflections, and the FWHM values of the $2\theta - \omega$ scan for the symmetric 002 and for the asymmetric 105 reflections are measured. Table 2. Gives the FWHM for the GaN samples (A, B, and F).

Table 2. The (FWHM) from the samples (A, B, and F).

Sample	Thickness (Å)	0002 ω -scans (arcsec)	0002 $2\theta - \omega$ scans (arcsec)	105 ω -scans (arcsec)	105 $2\theta - \omega$ scans (arcsec)
A	1000	0.12684	0.01015	0.06564	0.12684
B	2000	0.11624	0.01853	0.06201	0.04953
F	30μm	0.21557	0.00407	0.11647	0.02424

The broadening in the rocking curves is due to structural defects in the samples. When growing on sapphire the lattice and thermal mis-match between the GaN and sapphire induce a stress in the material, which causes the “a” and “c” lattice parameters to be strained. This strain was obtained by measuring the θ angle, calculating the “a” and “c” values and comparing the result with values from strain free materials (bulk GaN). The obtained values are given in table 3. The lattice strain along the “a” axis obtained from mathematical formula (4).

$$\varepsilon_{xx} = \varepsilon_{yy} = \frac{a - a_0}{a_0} \quad \text{and} \quad \varepsilon_{zz} = \frac{c - c_0}{c_0} \quad (4)$$

Where ε_{xx} is the in-plane strain components and ε_{zz} is the strain component in the z-direction. “a” and “c” are the strained lattice parameters, a_0 and c_0 are unstrained bulk lattice parameters of GaN.

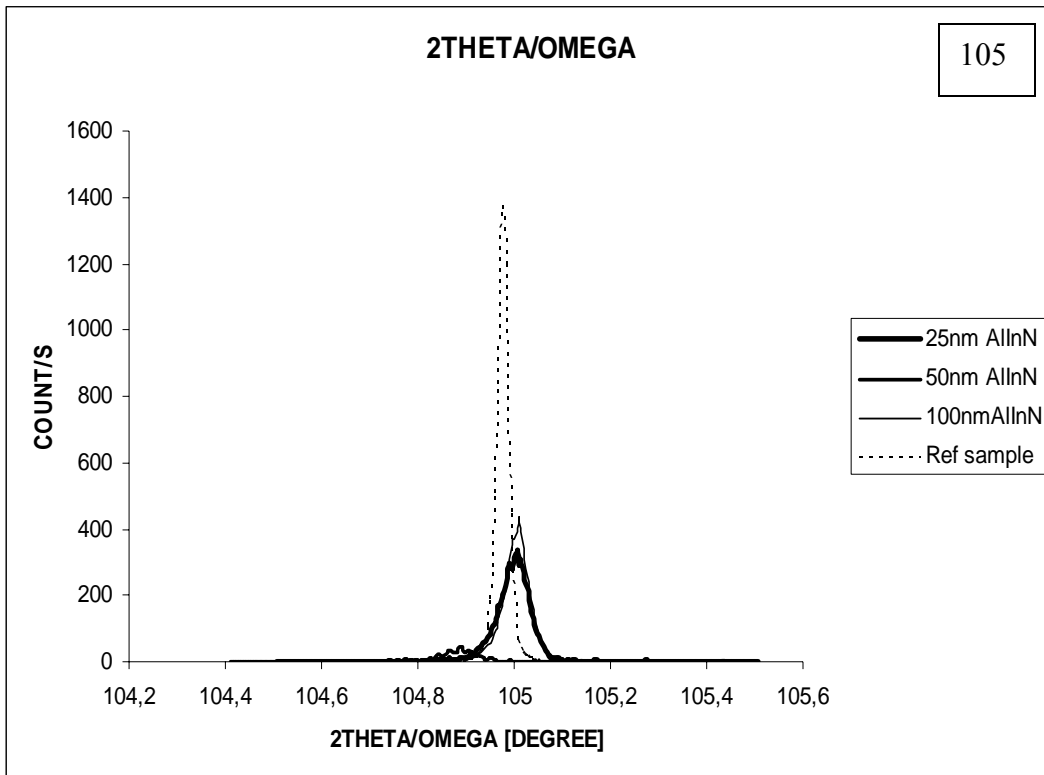
Table 3. The a and c lattice parameters, extracted from the GaN (1 0 5) and (0 0 0 2) peaks positions, the strain measured for the tow GaN samples

Sample	c (Å)	a (Å)	ε_{xx}	ε_{zz}	$\varepsilon_{xx} \%$	$\varepsilon_{zz} \%$
A	5.1923	3.1914	4.3887×10^{-4}	4.4316×10^{-4}	0.04439	0.0443
B	5.2066	3.1476	-0.0133	3.1985×10^{-3}	1.3291	0.3198
F	5.1916	3.1910	3.1348×10^{-4}	3.0829×10^{-4}	0.0313	0.0308

The results show that the lattice mis-match between sample A and the GaN is very small comparing with sample B, this causes less strain in sample A (strain components in both directions (x and y) are less in sample A comparing with sample B).

5.2.2 XRD measurements on samples grown by using only N₂ as carrier gas

The same XRD measurements were done for the GaN samples grown by using only N₂ as a carrier gas during the growth. The omega scans and 2 theta/omega scans for the 105 and 002 reflections are shown in Fig. 6.



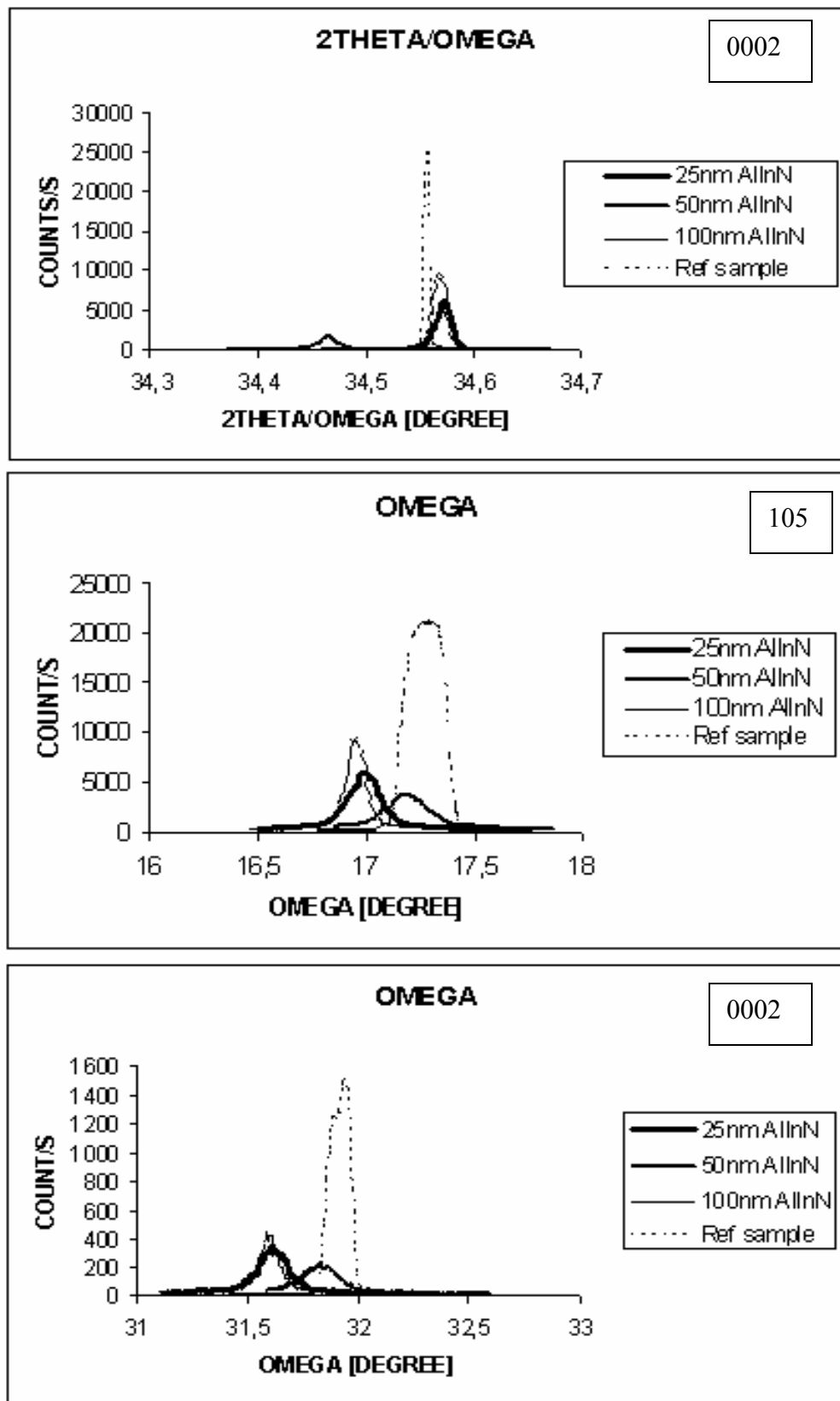


Fig. 6 The scans for the GaN samples grown by using only N_2 .

The FWHM values of the $2\theta - \omega$ scan for the asymmetric 0002 and for the symmetric 105 reflections are measured for the four GaN samples (C, D, E, and F). Table.4.

Table.4.The (FWHM) from samples (C, D, E, and F).

Sample	0002 ω -scans (arcsec)	0002 $2\theta-\omega$ scans (arcsec)	105 ω -scans (arcsec)	105 $2\theta-\omega$ scans (arcsec)
C	0.17643	0.01623	0.014992	0.06434
D	0.24558	0.01916	0.18748	0.18748
E	0.10691	0.01352	0.10299	0.04962
F	0.21557	0.00407	0.11647	0.02424

As a result from optical microscope, the samples show micro cracks, which are formed during the growth or at cooling down after the growth. Cracks influence the ω -scans and contribute to the wide range in numerical values observed. Dislocation generated at the interfaces between the sapphire substrate and the TiN and between the AlInN and the GaN, the domain width, and the sample bending also contributes to broadening of the rocking curves. The results show that the width of the ω -scans for the different GaN samples can be large and vary between (0.014992 and 0.18748) for 1 0 5 rocking curve and between (0.10691 and 0.24558) for 00 0 2 scan.. Sample (E) has less values of FWHM.

The strain again obtained by measuring the θ angle, calculating the “a” and “c” values and comparing the result with values from strain free materials (bulk GaN). The obtained values are given in table. 5.

Table. 5. The “a” and “c” lattice parameters, extracted from the GaN (1 0 5) and (0 0 0 2) peaks positions, and the strain measured for the GaN samples (C, D, E, and F).

Sample	C(Å)	A (Å)	ϵ_{xx}	ϵ_{zz}	$\epsilon_{xx} \%$	$\epsilon_{zz} \%$
C	5.1896	3.1948	$1.5047*10^{-3}$	$-7.707*10^{-5}$	0.1505	-0.0077
D	5.2041	3.1487	-0.0129	$2.717*10^{-3}$	-1.2947	0.2717
E	5.1898	3.1947	$1.4734*10^{-3}$	$-3.8536*10^{-5}$	0.1473	-0.0039
F	5.1916	3.1910	$3.1348*10^{-4}$	$3.0829*10^{-4}$	0.0313	0.0308

The strain components in both x and y directions is much smaller for sample E comparing with the other two samples C and D.

The values of the strain are not conclusive and it needs more depositions and XRD measurements to deduced quantitative information for a larger amount of experiment.

To investigate more information about the crystal quality, reciprocal space maps of the GaN samples grown on 100nm AlInN seed layers and the reference sample were taken around 002 and 105 reciprocal lattice points. Fig. 7 And Fig. 8 The Q_x and Q_y defined Q axes are given as reciprocal lattice units (rlu) $\times 10000$ by:

$$d_{rlu} = \frac{\lambda}{2Q_{RLU}}$$

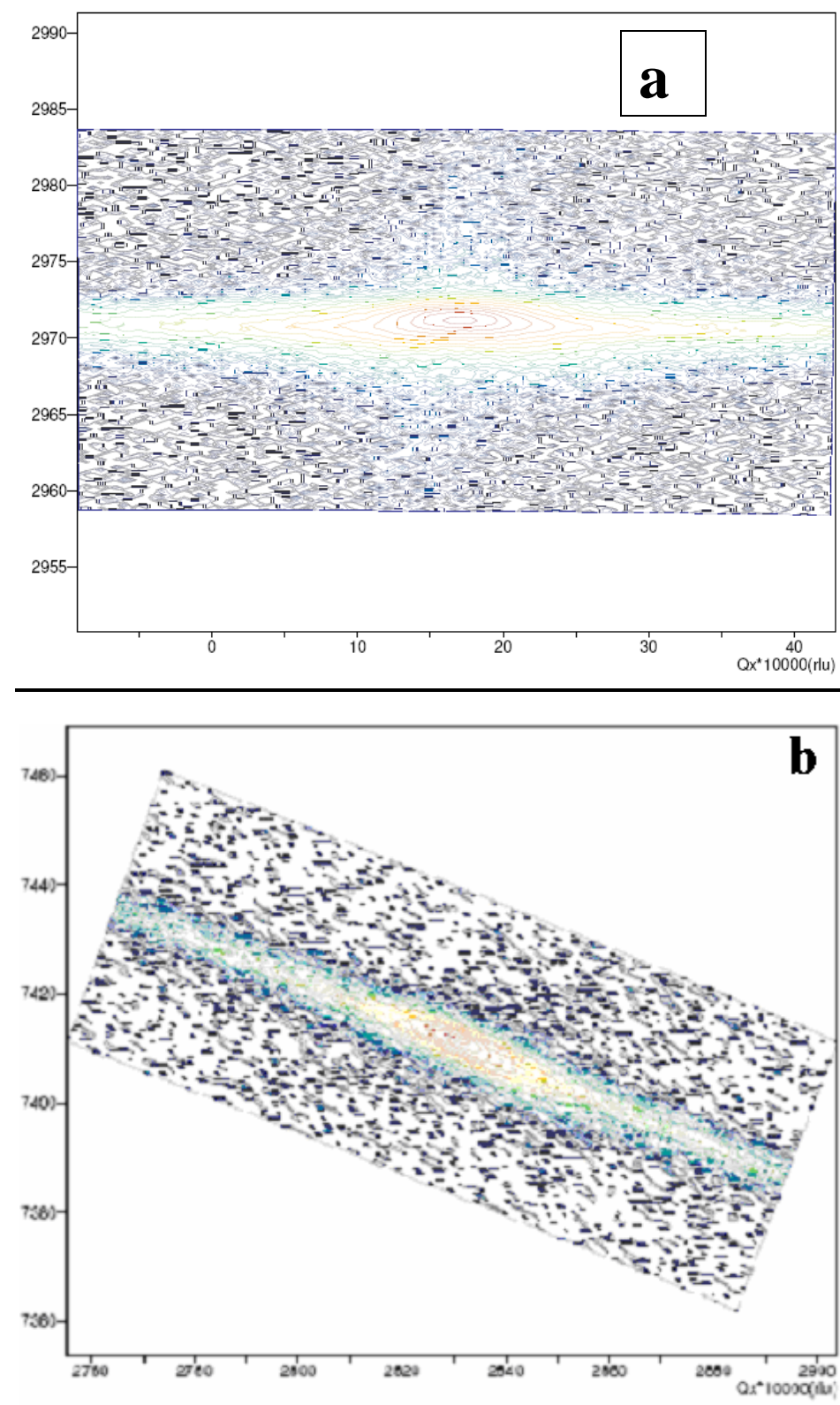


Fig.7 Reciprocal space map around (a) 0002 and (b) 105 points for samples (E)

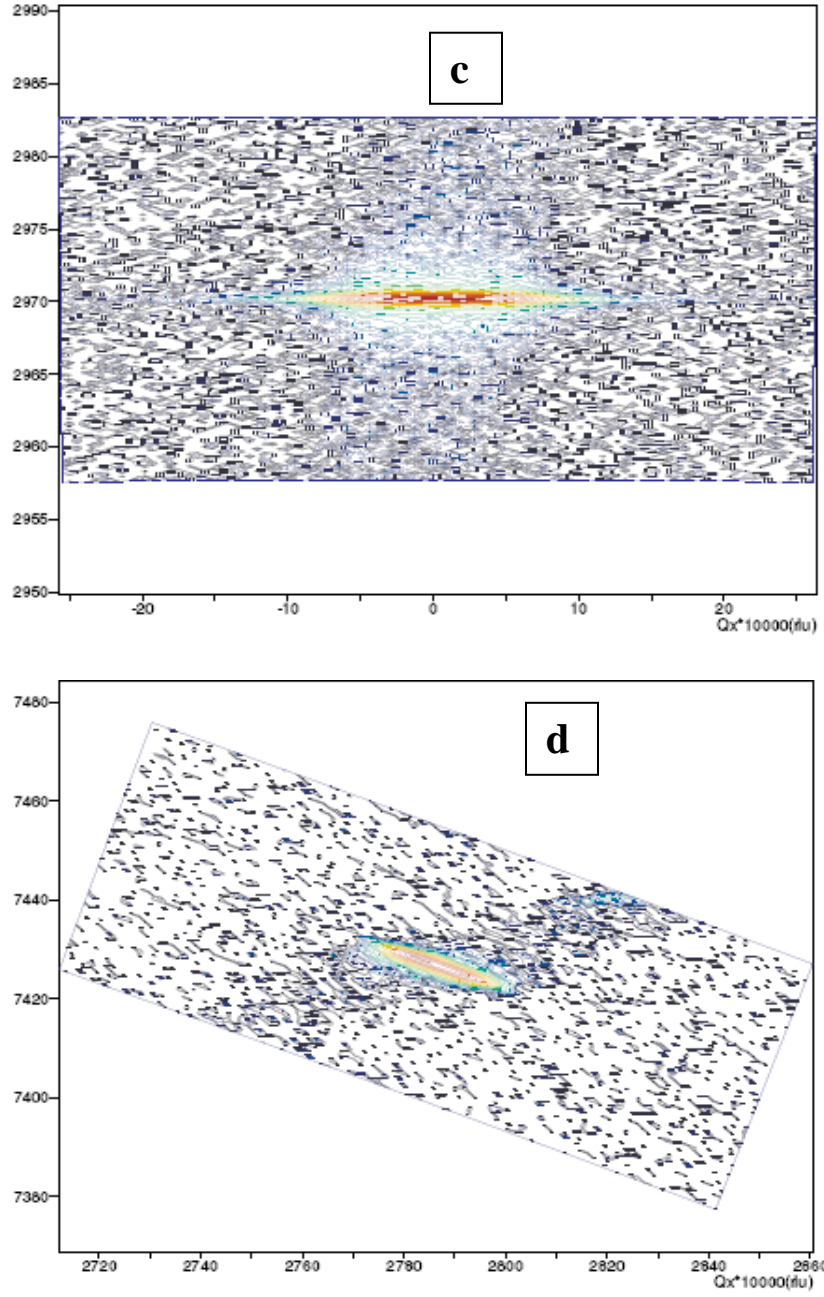


Fig. 8 Reciprocal space map around (c) 0002 and (d) 105 points for samples (F).

By looking at the RSM for sample (E) around the 002 point, we could see a considerable broadening in the direction parallel to the surface plane (ω direction) Fig.7 The broadening is also appear when we look at RMS around 105 reciprocal space point in direction that not parallel to the surface plane (ω direction). The FWHM for ω direction gives a lot of information about the crystalline quality, The broadening in RSM indicates an increase of either mosaicity or high density of dislocations [5.4], it can also be due to bending of the sample, which may be the case here since we know that large stresses are involved. Many types of dislocation can be found in the sample such as, misfit dislocation that comes from the lattice mis-match, etching dislocation, which it might come from the H₂ that was used in the chemical reaction during the growth of GaN.

The RMS shows broadening in the $(2\theta-\omega)$ direction perpendicular to (ω direction). Broadening of the $2\theta-\omega$ peak occur when there is a variation of the lattice parameters.

RMS for the reference sample around 002 and 105 points are given in Fig.8 Comparing with sample (E), a narrower peak in the ω direction and $(2\theta-\omega)$ are shown clearly, which indicates that the reference sample has less structural defects, the lattice parameters are well defined, and it has a high crystalline quality.

5.3 High resolution transmission electron microscope (HRTEM) results

The microstructure of GaN film was further evaluated by TEM. TEM sample preparation is very time consuming and expensive most of the time. It becomes even more difficult for those samples that have cracks in the grown films. So in order to save time and resources, TEM samples were prepared only for two samples out of six. The sample E and F was selected for this purpose and cross-sectional TEM samples were prepared.

Fig. 9 shows overview of the GaN film grown on AlInN / TiN / sapphire substrate and their interfaces. The growth rate of TiN and AlInN layers were calculated from X-rays reflectivity measurements and 500Å thick TiN buffer layer and 1000Å thick AlInN seed layer was grown. It is clear from the overview that the thickness of AlInN layer is roughly twice that of TiN layer confirming the relative growth rates. This GaN film is seen to have a large density of threading dislocations close to the interface which generally decreases further up in the film.

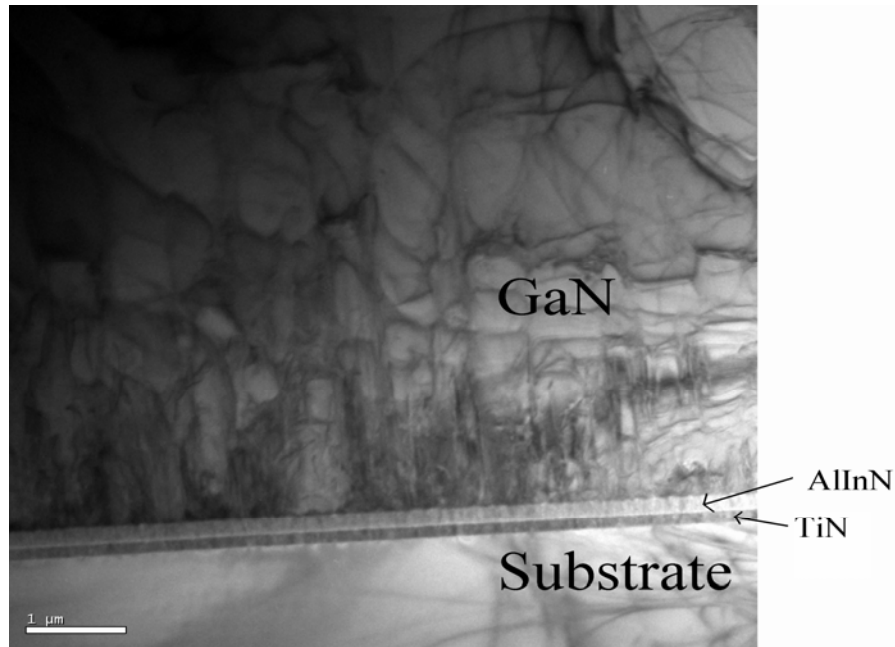


Fig. 9 cross sectional TEM micrograph showing overview of GaN film grown on AlInN/TiN/ sapphire.

Fig. 10 shows microstructures of GaN/AlInN/TiN/sapphire with higher magnification. The atomic number contrast of different layers can be clearly seen in this micrograph. The TiN buffer layer was darker than the $\text{Al}_{0.81}\text{In}_{0.19}\text{N}$ seed layer because the Ti is a heavier element than Al. The GaN film has darker contrast than TiN buffer layer because Ga is heavier element than Ti. The microstructure of layers and interfaces are very clear in this micrograph. This micrograph shows an abrupt interface between the sapphire substrate and the TiN buffer layer and is highlighted by the drawing box “a” in the Sapphire/TiN interface. This very sharp interface shows good epitaxy, no roughness mechanism and have no strain field in the substrate. There is also a sharp interface between TiN and AlInN seed layer highlighted by the drawing box “b” in the TiN/AlInN interface. Some voids can be seen near the interface and in the AlInN seed layer that are highlighted by drawing small circles on the AlInN seed layer. A very rough interface can be seen between the AlInN/GaN as is highlighted by the drawing box “c” in the interface region. This very rough AlInN surface may be due to etching in the CVD process. Some defects can be seen generated at GaN/AlInN interface that are travelling deep in the GaN. Similarly some defects are generated at TiN/AlInN interface that are also travelling deep in to the GaN film. Even more, some defects are generated at TiN/ sapphire interface travelling through seed layer and leading to GaN film. In short we can say that defects generated in different films and interfaces are travelling up to GaN film. None of the layer was capable to block the defects. Drawing lines on the layers highlight some of these defects. This causes a high defect density in the grown GaN film.

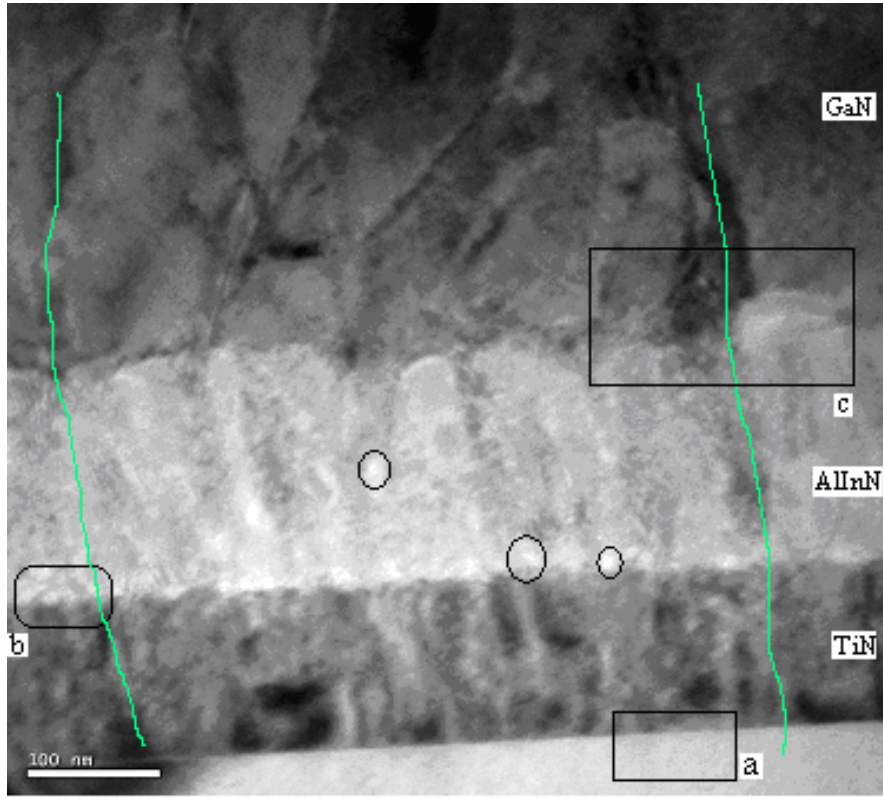


Fig. 10 high magnification cross sectional TEM micrograph of GaN/AlInN/TiN/sapphire

Fig. 11 shows an overview of the reference HVPE GaN film grown on MOCVD grown GaN buffer layer on sapphire substrate. The sharp interface between MOCVD grown GaN and sapphire substrate with little darker contrast with sapphire substrate and HVPE grown GaN is highlighted in the

area inside the circle. The darker contrast in the MOCVD grown GaN layer is due to trapping of large number of defects that are not propagating to HVPE GaN. The MOCVD grown GaN layer is serving as defect trapping layer. The GaN grown on AlInN seed layer have ten times more defects than reference sample (HVPE GaN grown on top of MOCVD grown GaN buffer layer).

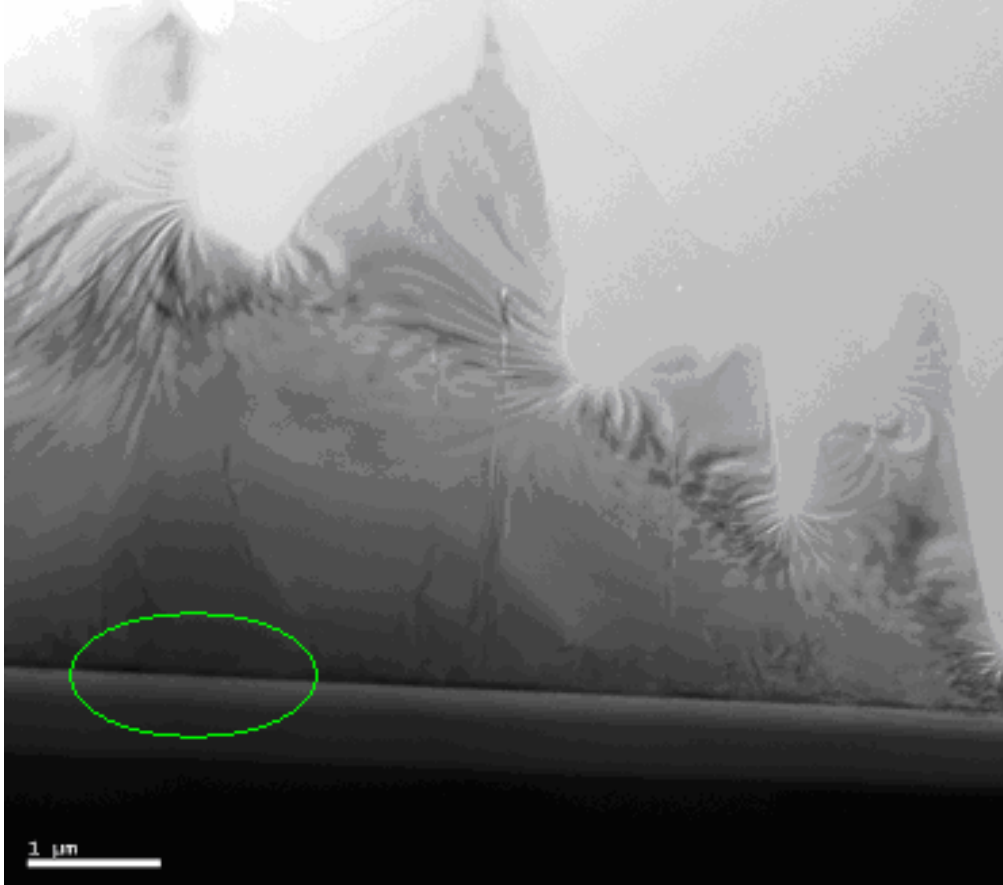


Fig. 11 cross sectional TEM micrograph showing overview of GaN film grown on sapphire by using MOCVD grown GaN seed layer

Fig. 12 is a high magnification image of the HVPE GaN grown on MOCVD grown GaN buffer layer. A sharp interface between MOCVD grown GaN and sapphire substrate can be seen more clearly in the highlighted area by the box that shows good epitaxy between MOCVD grown GaN and sapphire substrate. The white contrast that can be seen between the GaN buffer layer and the sapphire substrate shows strain in the sapphire substrate. The MOCVD grown GaN buffer layer shows a dark contrast with HVPE grown GaN shows due to a high density of structural defects in the MOCVD grown GaN buffer layer. It can be seen here that most of the defects were trapped in MOCVD grown buffer layer and were not propagating in HVPE GaN. A sharp interface between MOCVD grown GaN and HVPE grown GaN is also highlighted by a circle shows good epitaxy between the two layers.

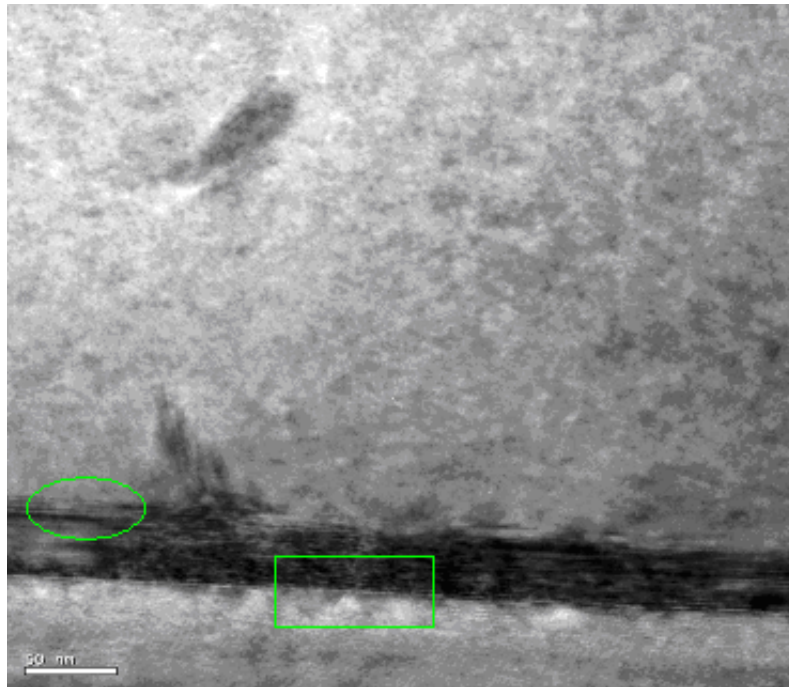


Fig. 12 high magnification cross sectional TEM micrograph of GaN film grown on sapphire by using MOCVD grown GaN seed layer

We can summarised our TEM results by saying our grown film have ten times more structural defects than the reference sample. In case of reference sample most of the defects are trapped in MOCVD grown GaN buffer layer while in case of our grown sample structural defects are travelling from substrate, TiN buffer layer and AlInN seed layer to the GaN film. A strain can be seen in sapphire substrate in case of reference sample that is not present in our grown sample. More over, we can say that our all TEM results are in quantitative agreement with the XRD results.

5.4 Cathode luminescence (CL) and SEM results

To understand the optical properties of HVPE grown GaN in relation with the morphology and crystalline quality, CL and SEM measurements were performed. On the basis of used carrier gasses, the measurements were divided in to two parts.

5.4.1 CL and SEM measurements on samples grown by using a mixture of N₂ and H₂ as carrier gas

Fig. 13 shows SEM images of the surface of the GaN (a) sample A (b) sample B and (c) sample F. The magnification and working distance of SEM was 3.00 KX and 12 mm respectively. The SEM image was taken with an accelerating beam energy of 10 KV. The SEM micrograph shows that the surface of GaN in very rough in sample A and B due to large number of big pits on the sample surface. In comparison, the surface of sample F is very smooth but some features can be seen on the surface.

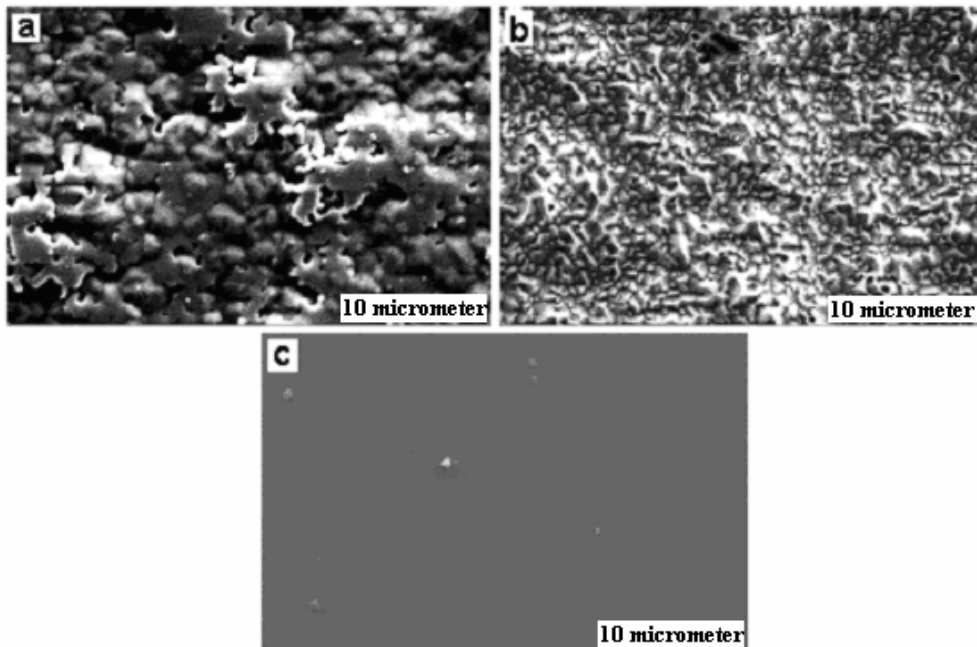


Fig. 13 SEM micrograph (a) surface microstructure of sample A. (b) surface microstructure of sample B. (c) surface microstructure of reference sample.

Fig. 14 shows panchromatic CL images of the surface of the GaN in the same area as the SEM images. (a) Sample A, (b) sample B and (c) sample F. The magnification and working distance of panchromatic CL was 3.00 KX and 12 mm respectively. The CL image was taken with accelerating beam energy of 10 KV. The panchromatic CL measurements are taken at liquid helium temperature. The bright areas show luminescence and dark areas have no luminescence and serving as contrast. Panchromatic CL shows large density of defects. These defects are so high in number that one cannot count them easily. Due to poor morphology, it is difficult interpret and drawing any conclusions concerning the dislocation density.

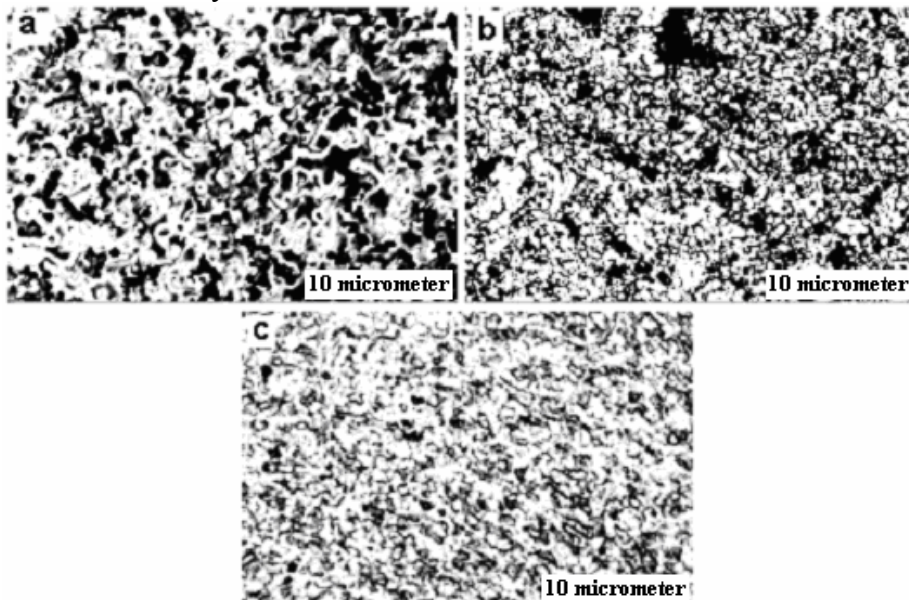


Fig. 14 Panchromatic CL image (a) CL image of sample A. (b) CL image of sample B. (c) CL image of reference sample.

Fig. 15 shows CL spectra's of the surface of the GaN. Donor bound exciton peaks are found at 357 nm, 360 nm and 358 nm for sample A, B and F respectively. The FWHM of CL spectra's are 43.76 mev, 102.52 mev and 14.57 mev for sample A, B and F respectively. The broadening of peaks show fluctuations of stress in case of sample A and B. This is due to a very poor surface morphology. The sample A and B shows very broad emission. This very broad emission can be explained by a high impurity concentration in the GaN film due to decomposition of AlInN seed layer because of etching effect of hydrogen gas that was used as a carrier gas.

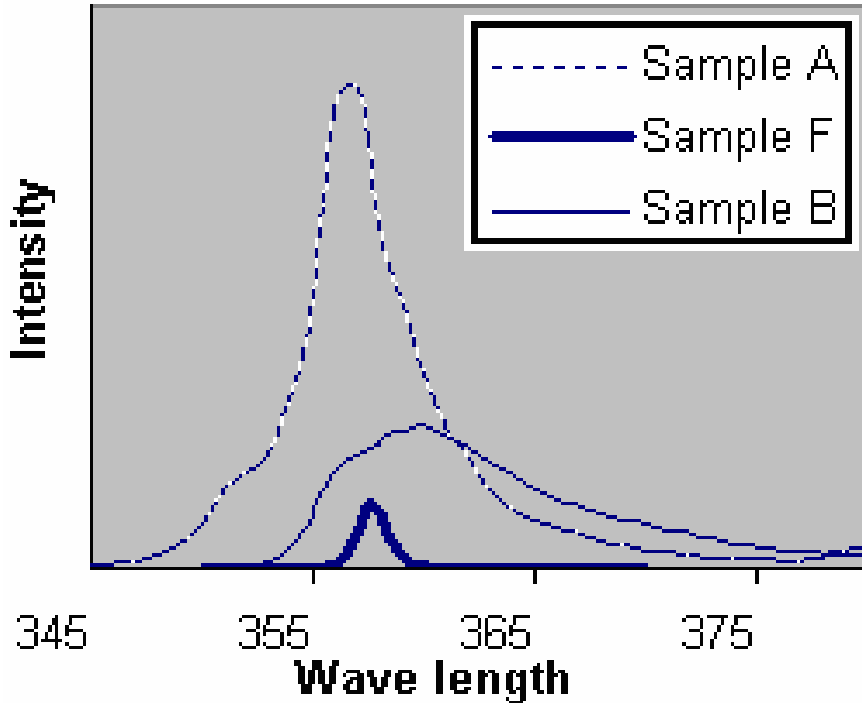


Fig. 15 Spectra's of CL for sample A, B and F.

5.4.2 CL and SEM measurements on the samples grown by using only N₂ as carrier gas

Fig. 16 shows SEM images of the surface of the GaN samples. (a) Sample C, (b) sample D, (c) sample E and (d) sample F. The magnification and working distance of SEM was 10.00 KX and 13 mm respectively. The SEM image was taken with accelerating beam energy of 5 KV. The SEM micrograph shows some features on the sample surfaces. It is to be noted that these surface features are non-uniform across the surface area of the samples. Some of these features are very small and some are so close to each other that they tend to overlap. So, it is difficult to determine their exact density. The density of these surface features in sample D seems to be higher than sample C. The density of surface features in sample E seems less compared sample C and D but very high as compared to sample F. These surface features have corresponding dark spot on a CL panchromatic map that are coming from non-radiative electron hole recombination centres. The dark spot density in CL image is higher than surface features that can be seen in the SEM. Thus CL reveals more dislocations than SEM.

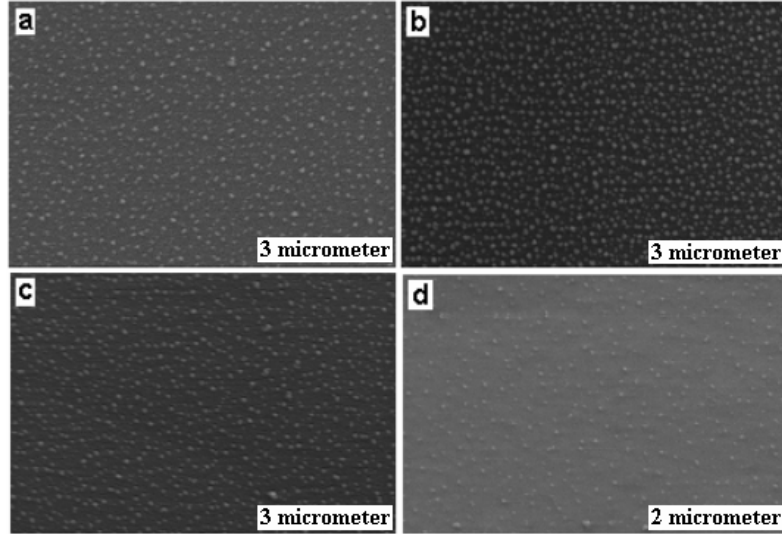


Fig. 16. SEM micrographs (a) surface microstructure of sample C. (b) surface microstructure of sample D. (c) surface microstructure of sample E. (d) surface microstructure of reference sample.

Fig. 17. shows panchromatic CL images of the surface of the GaN samples. (a) sample C, (b) sample D, (c) sample E and (d) sample F. The magnification and working distance for CL panchromatic map was 10.00 KX and 13 mm respectively. The CL panchromatic map was taken by using accelerating beam energy of 5 KV. The CL panchromatic map was taken at liquid helium temperature. The bright areas show luminescence and dark areas have no luminescence and serving as contrast. In bright regions radiative process dominates over non-radiative process because of lower density of structural defects. There are many dark spots in the CL map in the GaN epilayer. It can be seen that dark spots are non-uniformly distributed in all samples. The dark spots of CL map have close relation with the surface features of SEM image. Some small surface features in SEM are hard to distinguish but they have strong dark contrast in the CL image. At the same time, accuracy of CL mapping start to degrade due to coalescence of the dark contrast where some defects are too close to each other. Since dark spots tends to overlap to each other. It is very difficult to determine their exact density. A rough estimation gives a dark spot density for sample C and F about $3 \times 10^8 \text{ cm}^{-2}$. Just looking at CL map, we can say that dark spot density in sample D and E was about ten times higher than sample C and F.

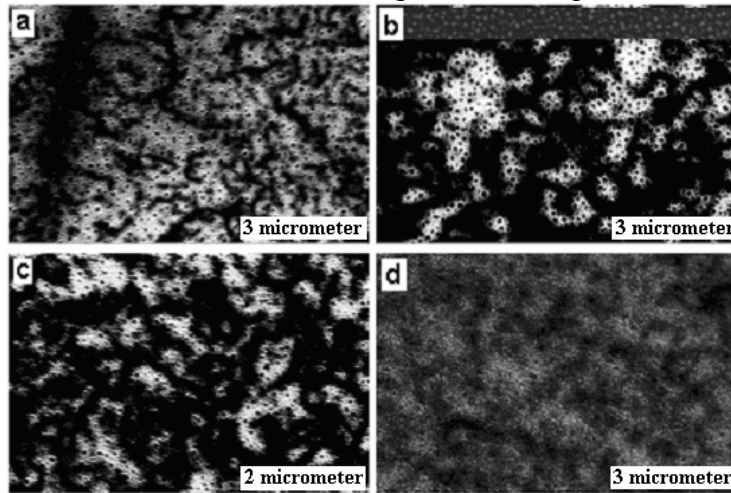


Fig. 17. Panchromatic CL images (a) CL image of sample C. (b) CL image of sample D. (c) CL image of sample E. (d) CL image of reference sample.

Fig. 18. Shows CL spectra's of the surface of the GaN. Donor bound exciton peaks are found at 357 nm, 356.5 nm, 357.5 nm and 356.5 nm for sample C, D, E and sample F respectively. The FWHM of CL spectra's are 16.99 mev, 22.00 mev, 14.50 mev and 14.57 mev for sample C, D, E and sample F respectively. The broadening of peaks show fluctuations of stress in the material. The sample D and F shows blue shifted donor bound exciton emission peak which shows biaxial compressive stress in the GaN film. The sample C and E shows donor bound exciton emission peak position at 357 nm and 357.5nm respectively. The stress is less in sample C and E since blue shift is less.

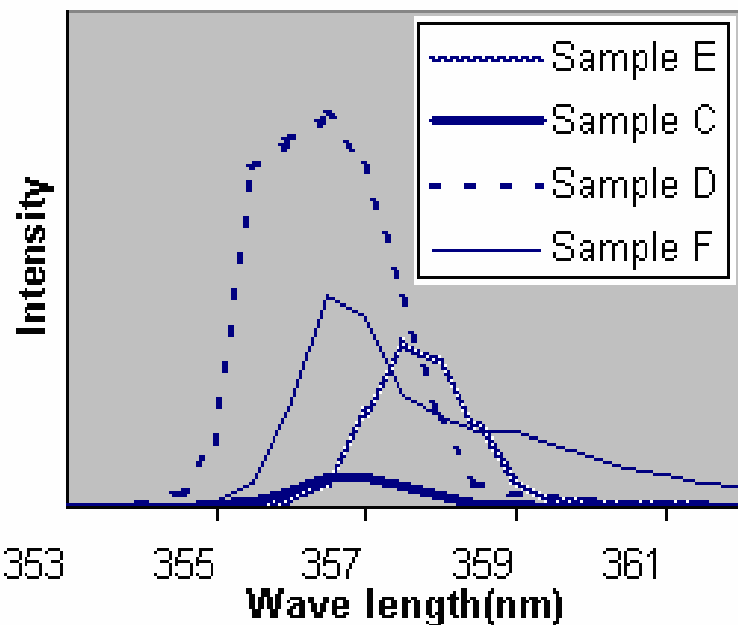


Fig. 18. Spectra's of CL of sample C, D, E and F.

Chapter 6: Conclusions

- The OM images of the GaN samples that were grown by using a mixture of H₂ and N₂ as a carrier gas shows very poor surface morphology and a very poor quality of the GaN as compared to the reference sample.
- The OM images of the GaN samples that were grown by using only N₂ as a carrier gas shows formation of cracks in the GaN films due to biaxial compressive stress. The concentration of the cracks varies between the samples and can be correlated with the thickness of the seed layer.
- The HRXRD measurements of the GaN samples that were grown by using mixture of H₂ and N₂ as a carrier gas shows very high structural defects and strain in the lattice parameters. The values of the strain are not conclusive and scattered in strange way. More XRD measurements are needed to deduced quantitative informations.
- The HRXRD measurements of the GaN samples that were grown by using only N₂ shows also strain in the samples. The information obtained from RSM (reciprocal space map) indicate high density of structural defects and variation in lattice parameters as compared to reference sample that have less structural defects and well defined lattice parameters.
- TEM sample preparation is time consuming and expensive most of the time. So in order to save time and resources. Only one of the best sample which was grown by using only N₂ as a carrier gas and the reference sample was selected for TEM. The HRTEM micrograph shows that our grown sample has ten times more structural defects than the reference sample. A strain can be seen in substrate in case of the reference sample that is not present in our grown sample. These HRTEM results are in qualitative agreement with the HRXRD and CL measurements.
- The SEM micrographs and CL panchromatic images of the GaN samples that were grown by using mixture of H₂ and N₂ as a carrier gas shows very poor surface morphology and very high defect density as compared to the reference sample. Due to poor morphology, it is difficult to interpret and drawing any conclusions concerning the defect density. The CL spectra's shows broadening of peaks due to fluctuant of stress, from bad morphology and a high impurity concentration possibly from a decomposed AlInN seed layer.
- The SEM micrographs and CL panchromatic images of the GaN samples that were grown by using only N₂ as a carrier gas shows surface features in SEM micrograph having corresponding dark spot on a CL panchromatic map. The dark spot density in CL image is higher than surface features in the SEM micrograph. CL reveals more dislocations than SEM. A rough estimation gives a dark spot density for our grown sample about 10⁸ cm⁻² that was about ten times higher than the reference sample. The CL spectra's shows blue shifted donor bound exciton emission peaks due to biaxial compressive stress in the GaN film. The SEM and CL results are in qualitative agreement with the XRD and HRTEM results.

Chapter 7: References

Chapter 1: Introduction

- [1.1] Aldo Mele, Anna Giardini, Tonia M. Di Palma, Chiara Flamini, Hideo Okabe, and Roberto Teghil, International Journal of Photoenergy, 2001
- [1.2] Vanya Darakchieva, Strain-related structural and vibrational properties of group –III nitride layers and superlattices, Dissertation No. 891, Linkoping University Press, 2004.
- [1.3] Bilge Imer, Improved Quality Non-polar III-Nitride Heteroepitaxial Films and Devices, Dissertation, University of California, December 2006
- [1.4] Timo Seppänen, Growth and Characterization of Metastable Wide and-gap AlInN Epilayers, Dissertation No. 1027, Linkoping University Press, 2006, ISBN No: 91-85523-58-5.
- [1.5] Rafal R.Ciechonski, Growth and characterization of SiC and GaN, Dissertation No.1151, Linkoping University Press, 2007.
- [1.6] Qixin Gue, Kousuke Yahata, Tooru Tanka, Mitsuhiro Nishiro, and Hiroshi Ogawa, phys. Stat. sol.(c) 0, NO. 7,2533-2536 (2003).
- [1.7] Jens Birch, Sukkaneste Tungasmita and Vanya Darakchieva, Vacuum Science and Technology (2002) 421-456.
- [1.8] Q.X. Gue, Y. Okazaki, Y. Kume, T. Tanaka, M. Nishio, H. Ogawa, Journal of Crystal Growth 300 (2007) 151-154, 2006.
- [1.9] T. Seppanen, G. Z. Radnoczi, Journal of Applied Physics 97, 083503, (2005)
- [1.10] Henrik Larsson, Growth of Thick GaN Layers on Sapphire by Hydride Vapour Phase Epitaxy, Dissertation No. 958, Linkoping University Press, 2005.
- [1.11] Milton Ohring, Material Science Of Thin Films, Academic Press, 525 B Street, Suit 1990, San Diago. USA, 2002.

Chapter 2: Growth Techniques

- [2.1] Milton Ohring, Material Science Of Thin Films, Academic Press, 525 B Street, Suit 1900, San Diego, USA, 2002.

[2.2] Jens Birch, Sukkaneste Tungasmita and Vanya Darakchieva, Vacuum Science and Technology: Nitrides as seen by the technology, 421-456. (Research signpost, Kerala, 2002)

[2.3] Timo Seppänen, Growth and Characterisation Of Metastable Wide Band Gap AlInN Epilayers, Dissertation No.1027, Linköping University Press, 2006, ISB Number 91-85523-58-5.

[2.4] V S Ban, J Electrochem Soc 119 (1972) 761

[2.5] C.E.C. Dam, A.P. Grzegorczyk, P.R. Hageman and P.K. Larsen, Journal of Crystal Growth, Volume 290 (2006) 473-478

[2.6] H. M. Kim, J. E. Oh, T. W. Kang, Materials Letters, Volume 47 (2001) 276-280.

[2.7] Detchprohm, T, Hiramatsu, K, Amano, H and Akasaki, 1992, Appl. Phys.Lett, 61, 2688.

[2.8] Henrik Larsson, Growth of thick GaN layers on Sapphire by Hydride Vapour Phase Epitaxy, Dissertation No.958, Linköping university press 2005, ISBN-No: 91-85299-75-8

[2.9] C. Hemmingsson, P. P. Paskov, G. Pozina, M. Heuken, B. Schineller and B. Monemar, Super lattices and Microstructures, 40, (2006) 205-213

[2.10] V S Ban, Journal of crystal growth 17, (1972), 19-23

[2.11] E. Richter, Ch.Hennig, M. Weyers, Journal of Crystal Growth 277, (2005), 6

Chapter 3: Characterisation Techniques

[3.1] Cullity, B.D and Stock, S.R., Elements of x-ray diffraction, 3rd.ed.Prentice Hall, Inc., New Jersey (2001).

[3.2] Laboration compendium, X-Ray Diffraction (XRD), Linköping University.

[3.3] Hard P.Klug Leroy E.Alexander, X-Ray Diffraction procedures for polycrystalline and amorphous materials, 2nd. Ed. (1974).

[3.4] Jens Birch, Laboration compendium, Laue Camera, Linköping University.

[3.5] Timo Seppänen, Growth and Characterisation of Metastable Wide Band Gap AlInN Epilayers, Dissertation No.1027, Linköping University Press, 2006

[3.6] Laboration compendium Transmission Electron Microscopy (TEM), Linköping University,

[3.7] McCaffrey, John P., Development of Transmission Electron Microscopy Techniques for the Study of Thin Films, Dissertation No.631, Linkoping University Press. (2000).

[3.8] Holt, D.B and Joy, D.C, SEM Microcharacterization of Semiconductors, Academic Press Inc. (1989).

Chapter 4: Experimental details and characterisation of $\text{Al}_{1-x}\text{In}_x\text{N}$ seed layer

[4.1] Richard C. Jafer, Introduction to microelectronic fabrications, 2nd Edition, Volume V, Prentice Hall, Upper saddle river, New jersey 07458 USA, 2002.

[4.2] T. Seppänen, M. Beckers, U. Kreissig, L. Hultman, and J. Birch, J.Appl.Phys.101, 043519 (2007)

Chapter 5: Results And Discussions

[5.1] Timo Seppänen, Growth and Characterisation Of Metastable Wide Band Gap AlInN Epilayers, Dissertation No.1027, Linköping University Press, 2006, ISBN No: 91-85523-58-5.

[5.2] E. V. Etzkorn and D. R. Clarke, International Journal of High Speed Electronic and Systems, Vol. 14, No.1 (2004) 63-81.

[5.3] Henrik Larsson, Growth of Thick GaN Layers on Sapphire by Hydride Vapour Phase Epitaxy, Dissertation No. 958, Linkoping University Press, 2005, ISBN: 91-85299-75-8.

[5.4] 1- Jens Birch, Sukkaneste Tungasmitta and Vanya Darakchieva, Vacuum Science and Technology (2002) 421-456.